Distribution Agreement

In presenting this thesis as a partial fulfillment of the requirements for a degree from Emory University, I hereby grant to Emory University and its agents the non-exclusive license to archive, make accessible, and display my thesis in whole or in part in all forms of media, now or hereafter now, including display on the World Wide Web. I understand that I may select some access restrictions as part of the online submission of this thesis. I retain all ownership rights to the copyright of the thesis. I also retain the right to use in future works (such as articles or books) all or part of this thesis.

Benjamin F. Lonial March 31, 2023

Dynamics of 2-Dimensional Soft Particle Flow Through Hopper

By

Benjamin F. Lonial

Eric R. Weeks, PhD
Advisor

Physics

Eric R. Weeks, Ph.D.
Advisor

Thomas J. Bing, Ph.D.
Committee Member

Andrew J. Mitchell, Ph.D.
Committee Member

2023

Dynamics of 2-Dimensional Soft Particle Flow Through Hopper

By

Benjamin F. Lonial

Eric R. Weeks, Ph.D.

Advisor

An abstract of
A thesis submitted to the Faculty of the Emory College of Arts and Sciences
of Emory University in partial fulfillment
of the requirements for the degree of
Bachelor of Sciences with Honors

Physics

2023

Abstract

Dynamics of 2-Dimensional Soft Particle Flow Through Hopper
By Benjamin F. Lonial

I study the quasi-2d hopper flow of oil-in-water emulsions as they exit an orifice in two scenarios. First, I look at many particle flow of droplets with diameters smaller than the opening width For many particle flow, prior work on hopper dynamics has focused on the flow rate, which is defined as the number of oil droplets exiting per unit time. This has shown a general power law dependence between flow rate, Q, the ratio of the opening width, w, to the average diameter of droplet size, d, and the fitting constant κ as such: $Q \sim (w/d - \kappa)^{\beta}$. Prior work has seen various values for the exponent β, corresponding to different experimental conditions. Recent work has suggested that the range of values for the exponent β can explained by the ratio of the viscous drag force of particles moving in their medium to the kinetic friction of two particles sliding past each other. In two dimensions, for the low kinetic friction limit, this exponent should be 1/2. We experimentally verify this claim by studying the flow rate of silicon oil-in-water emulsions as they pass through an orifice over a range of w/d values. We find that the flow rate collapses to the general curve with $\beta = 0.49$ and $\kappa = 1.47$. I then extend this work to examine the flow of a oil droplet with a diameter larger than the opening width of the orifice. If the volume of oil is high enough, I find that droplets can flow through this opening by deforming, even when the droplet diameter is $3\times$ the size of the opening. In this scenario, I compare my results with the common approach to modelling soft particles: the Durian bubble model. This model predicts that once the droplet is half-way through the opening, the wall-droplet repulsion assists in pushing the droplet out of the hopper, so much so that the droplet overshoots its terminal velocity. I find that my experiment is unable to replicate the velocity overshoot predicted by the Durian bubble model. I suggest that this occurs because of a regime where viscous dissipation is capable of depleting the energy required to overshoot, as well as the presence of a non-negligible depletion force.

Dynamics of 2-Dimensional Soft Particle Flow Through Hopper

By

Benjamin F. Lonial

Eric R. Weeks, Ph.D.

Advisor

A thesis submitted to the Faculty of the Emory College of Arts and Sciences
of Emory University in partial fulfillment
of the requirements for the degree of
Bachelor of Sciences with Honors

Physics

2023

Acknowledgments

I would like to thank my advisor for this project Dr.Eric Weeks for supervising and letting me work on this project. I came into this lab with no background in soft matter and less ability in coding, and yet Dr.Weeks was able to teach me both, acquainting me with a side of physics that requires creativity and ignites exploration. In addition, thank you to the Emory physics and philosophy departments for its myriad of courses that allowed to me practice and develop the skills for thinking, and the room to explore the connections between these disparate courses. I would also like to thank my family, whose support enabled my interests to go unimpeded, and my friends, Jenna, Jeffrey, George, Kennedy, and Cole, whose perpetual presence and passion these past years has been motivation alone for my education. Finally, I would like to thank my roommate for reading everything I have written. I truly could not have done this without you. Also, funding for this project is provided by The National Science Foundation CBET-2002815.

Contents

1 Introduction **1**

1.1 Many Particle Flow and the Wandering Exponent 2

1.1.1 Beverloo Law 2

1.2 Single Particle Flow 5

1.2.1 Surface Tension 5

2 Methods **7**

2.1 Emulsion Production 7

2.1.1 Snap Off Through Direct Syringe Injection 10

2.1.2 Microfluidic Device 11

2.2 Chamber Design 14

2.2.1 Hopper Material 14

2.2.2 Hopper Initialization 17

2.3 Microscopy 18

2.4 Computational Work 19

2.4.1 Particle Tracking 19

2.4.2 Measuring Flux 20

3 Multiple Particle Results and Analysis **21**

3.1 Trajectory of Droplets 21

3.2 Velocity Profiles 23

3.3 Flux . . . 26
3.3.1 Flux for Soft Particles . . . 26
3.3.2 Experimental Data on Flux . . . 27
3.4 Fitting to the Beverloo Equation . . . 29
3.5 Summary of Findings . . . 32

4 Single Particle Results and Analysis **33**
4.1 Velocity . . . 33
4.1.1 Durian Bubble Model . . . 33
4.1.2 Surface Energy and Velocity . . . 39
4.1.3 Center of Mass Velocity . . . 39
4.1.4 Leading and Trailing Edge . . . 45
4.2 Summary of Findings . . . 48

Conclusion **48**

Bibliography **51**

List of Figures

1.1 Drawn image of hopper flow 1

2.1 Images of oil moving through hopper 8
2.2 Image demonstrating the danger of too much surfactant 9
2.3 Image demonstrating depletion effect 9
2.4 Snap-off procedure for droplet creation 11
2.5 Image of the set used to inject oil into hoppers 12
2.6 Images of three regions of microfluidic droplet production under a microscope 13
2.7 Images of three different chambers and emulsion techniques 15
2.8 Image taken of large droplet deliberately produced to clog opening 17
2.9 Image of imaging apparatus 18
2.10 Image taken from lblmovie.pro 19

3.2 Contour plot for ψ_6 21
3.1 Still image from hopper flow and trajectory of droplets over a 25 second range 22
3.3 A heat map representing the speed of droplets flowing through a hopper . . . 23
3.4 Velocity profiles of droplets filing through hopper 25
3.5 Two images of hopper flow under microscope 27
3.6 Graphs of flux as a function of the square root of remaining droplets and the Beverloo coefficients for a small range of fitting by means of ftfinder.pro . . . 28
3.7 Power Law Fitting of Beverloo Coefficients 30

3.8 Graph of the average vertical velocity, in pixels per second, of droplets against the height, in pixels, for a range of w/d 31

4.1 Geometry of single droplet flowing through hopper 34

4.2 Graph of normalised speed (velocity divided by terminal velocity) against timesteps for a single droplet flowing through hopper over multiple values of μ 37

4.3 Graphs of velocity and normalised perimeter for a single droplet flowing through hopper 40

4.4 Graph of velocity as a function of time for four different values of w/d 42

4.5 Consecutive image of droplet separating from wall 43

4.6 Speculation of velocity in the absence of depletion force 44

4.7 Graph of leading, trailing and center of mass velocity for two droplets 45

4.8 Graph of trailing edge velocity for three differently sized droplets 47

Chapter 1

Introduction

This investigation into the dynamics of soft particles is motivated by an aim to continue and expand research on the factors decisive in the phenomenon of soft particle flow in general. This means crafting experiments that tease out the subtle physics at stake, accentuating the features which lie dormant in our intuitive or computational presuppositions.

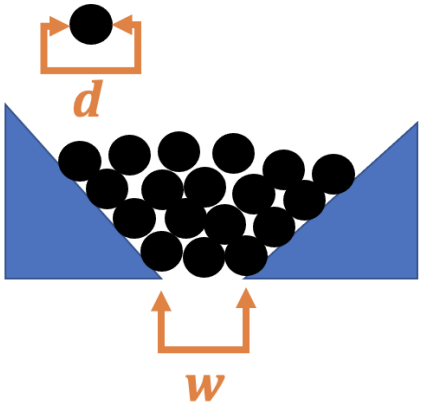

Figure 1.1: Drawn image of hopper flow. The constriction is a funnel that droplets are forced to flow through. The opening of the hopper is w and the diameter of droplets is d.

I conduct two such experiments and report their findings in this thesis. The first experiment looks at the hopper flow of many particles with diameters smaller than the orifice width, in the spirit of prior work done by Beverloo *et al.* [4]. Hopper flow is the phenomenon where discrete particles are forced to flow through a constriction, which I have sketched in Fig.1.1. The constriction forces the particles to interact with each other because there is a limit imposed on their ability to flow. Think, for instance, of grain draining through a silo. Many granular particles flow through an opening that is much larger than their average diameter, meaning that the constriction introduces *some* impedance, but not enough to commonly produce clogging. The question I look to examine is how soft, frictionless particles flow differently.

The second experiment I conduct inverts the first to examine one soft particle with a diameter larger than the opening width. If this were a hard particle, there would be no question about its ability to flow— the hard particle would make contact with the walls and not move any further. But, if the particle is soft and its weight great enough, it can flow through. What are the dynamics of this flow?

Both of these experiments are conducted with an eye towards two computational models: the Durian bubble model, suggested by Durian *et al.*, and the Deformable particle model (DP model), suggested by Boromand *et al.* [10, 5]. The specifics of these models will be discussed later. That said, my aim in this project is to bring into focus the behaviours of soft particle flow, particularly the features that might highlight a breakdown in our current computational models.

1.1 Many Particle Flow and the Wandering Exponent

1.1.1 Beverloo Law

One cannot talk about hopper flow without first citing Beverloo *et al.* [4]. It was there that a power law dependence was stated for the correlation between flow rate and the ratio between the opening width w to the average diameter d, as such:

$$W = C_m \rho_B \sqrt{g} \left(\frac{w}{d} - \kappa \right)^{2.5}. \tag{1.1}$$

Where W is the flow rate, ρ_B is the density of the flowing material, g is the acceleration of freely falling bodies, w is the opening width of the hopper, and d is average particle diameter. The first constant, C_m, is characterised by the material properties of the flowing particles (Beverloo measured this value for the curious assortment of sand, watercress, lupin, kale, swede and others), whereas the second constant, κ, measures the minimum ratio of w/d after which clogging occurs (since the flow rate goes to 0 as κd approaches w). Most work on

hopper flow has generally looked at the flow of hard particles (they do not deform) where friction is likely to dominate the dynamics of flow.

For these hard, frictional system, β traditionally has been correlated to the spatial dimension of the hopper (2-dimensional, 3-dimensional, etc.), scaling as $\beta = \text{dim} - 1/2$, where dim is the dimension. In two dimensions, this can be understood if we imagine droplets of diameter d flowing with uniform velocity v down an infinite length two dimensional hallway of width w. The flux of droplets is the number of droplets passing a certain position over a period of time: $\frac{dN}{dt}$. The maximum number of droplets that stack across is given by $N = w/d$. The time it takes one row of droplets to pass a certain threshold is the amount of time it takes droplets to fall their own diameter, i.e. $t = d/v$. The flux is given by $\frac{dN}{dt} = \frac{wv}{d^2}$. In a hopper, the velocity is approximated by saying that droplets within an area of $w \times w$ above the hopper fall freely, thus $v^2 \sim gw$, and the flux becomes $\frac{dN}{dt} \sim w^{3/2}$ (note that in 2-dimensions $2 - 1/2 = 3/2$). The argument is similar for three dimensions[7].

More recent work, however, has moved towards looking at the flow of soft, frictionless particles in order to understand how these properties affect the parameters within the Beverloo equation and hopper flow as a whole. In particular, prior work from the Weeks lab has shown how softness dips κ lower since softer particles can squeeze through more narrow openings [13]. Other groups have exposed have exposed deviations from the predicted value of β [16, 20, 14, 1]. Some have even cited exponents as curious as $\beta = 1$, which means that the experiment was theoretically conducted in 1.5-dimension chamber— something unphysical [11, 3, 21].

On the computational side, an approach to modelling droplets as circles which can overlap as a function of softness— called the Durian bubble model— but repel each other as a linear function of this overlap, have similarly troubled the strict dimensional dependence of β, exhibiting the presence of deviations [10, 17].

Since these particles are deformable and their effective diameter is smaller perpendicular to the direction of flow, we expect that softer particles can stack such that the maximum

number of droplets that can exit at a time is greater than w/d. That said, how might frictionless droplets tinker with the area of free fall? In a high viscosity fluids, droplets will reach terminal velocity (that velocity which makes squirrels immortal) quicker, resulting in a limit to the outgoing velocity. But, at the same time, is it fair to assume that *frictionless* droplets fall from a height w? In the end, is this enough to account for the deviation? Does this imply that hopper geometry is irrelevant to β, or does this simply call for a correction?

Another computational approach to this problem, from out of the O'Hern group, models droplets as polygons whose vertices are connected by springs [5, 6]. Recently, they have focused on the effects of the two key dissipative mechanism: viscous drag and kinetic friction. Dissipative forces are those forces which irrecoverably dissipate energy into the environment. The viscous drag force is a feature of droplets moving through a viscous fluid that resists fast moving droplets, like running in the ocean. The kinetic friction force is a force that resists strong variations in the overall range of speeds, so that two adjacent droplets are averaged to similar velocities (if you imagine yourself trying to run in a crowd, then kinetic friction is akin to how hard it is pass the person ahead of you).

This model suggests that β is determined by the relative strength of each mechanism. In the limit where viscous forces are negligible relative to kinetic friction, they reproduce the granular flow $\beta = \text{dim} - 1/2$, whereas the limit where viscous drag becomes more important than kinetic friction results in $\beta = \text{dim} - 3/2$. As such, if we are to study the flow of soft frictionless droplets, we should expect that the flow of droplets should fit to the exponent $\beta = 1/2$.

Similarities between this predicted exponent for frictionless particles and the granular systems is that any increase in w/d increases the flow rate. But, for a $\beta = 1/2$ exponent this flow rate increase starts to mean less as we go to higher w/d. Compare this to a $\beta = 3/2$ exponent where any increase in w/d means a great deal for the flow rate, and means *more* as we go to higher w/d. If frictionless particles do indeed flow according to a $\beta = 1/2$ exponent, then we expect for this payoff decrease to materialise in the flow patterns of the particles.

Ultimately, my aim is to measure the Beverloo exponent for soft frictionless particles and combine this measurement with information from the chambers in order to understand how this exponent materialises in the hopper patterns themselves.

1.2 Single Particle Flow

While the flow of many droplets through an orifice width greater than the average diameter can help us situate softer particles within the canonical understanding of hopper flow, we can also invert our experiment to understand more deformable droplets. After all, if we are studying soft particles in hoppers we would be remissed to ignore the very thing that makes them special— their softness.

1.2.1 Surface Tension

One crucial concept that stands in need of elucidation is surface tension. Surface tension arises from the imbalance of inter-molecular bonds at a boundary between two fluids. This results in a net force that tends to group fluids together such that the area of contact between the two fluids is minimised. Surface tension is essentially a statement by one fluid in contact with another that it wants the least amount of contact possible.

That said, surface tension must negotiate its wants within the economy of other energy considerations. Take, for instance, a single drop of water, which forms a neat hemisphere, against a puddle. In the drop of water, surface tension is able to preside more effectively and dominate the circular shape, whereas the puddle silences surface tension since other concerns, such as gravity, are more important.

For a droplet larger than the opening width, buoyancy pays energy to temporarily increase the surface tension of the droplet, so that the droplet deforms. This deformation allows the droplet to squeeze through the opening, ultimately allowing the passage of the droplet through the hopper, even though its diameter is larger than the opening width. As it turns

out, surface tension is the only reason that something soft can flow through an opening smaller than its diameter, without, of course, breaking the boundary of the droplet or the hopper altogether.

This ability to squeeze through narrow openings is one of the fascinating features of soft particle flow. This increased deformability also tests the limits of certain ways of thinking about these droplets. Namely, is the Durian bubble model, which was first developed to study the effect of shearing foams, a good way of modelling highly deformed droplets, or does something break down? Can the newer DP model, which can accurately model the shape of deformed droplets, accurately model the entire system? I aim to study more deformed droplets in this simple system as a way to simply test the physical features of soft particle flow.

Chapter 2

Methods

2.1 Emulsion Production

An emulsion is a mixture of two immiscible liquids, where one liquid is in a continuous "environment" phase and the other is suspended in this environment as discrete little droplets. That is to say, a layer of oil and a layer of water do not an emulsion make. But, when we shake a container with oil and water, the big layer of oil is separated into smaller oil bubbles of various sizes— this is now an emulsion. After a period of time, a shaken bottle of pure water and oil will eventually settle back into its original layered de-composition. This occurs because it is energetically favorable for two small droplets to coalesce into one big one, since this decreases their surface area per unit volume.

While emulsions occur in many of our everyday food items such as milk and mayonnaise, for our purposes here, emulsions are appropriate because they model soft, deformable, frictionless particles.

Traditional hopper flow experiments tend to focus on hard particles, which can clog by forming strong arches. Soft particles, because of their deformability, are able to pack more tightly, and thus occupy cracks hitherto inaccessible to hard particles, thus allowing more acrobatic flow dynamics. To get a sense of this, compare the three images in Fig.2.1 all

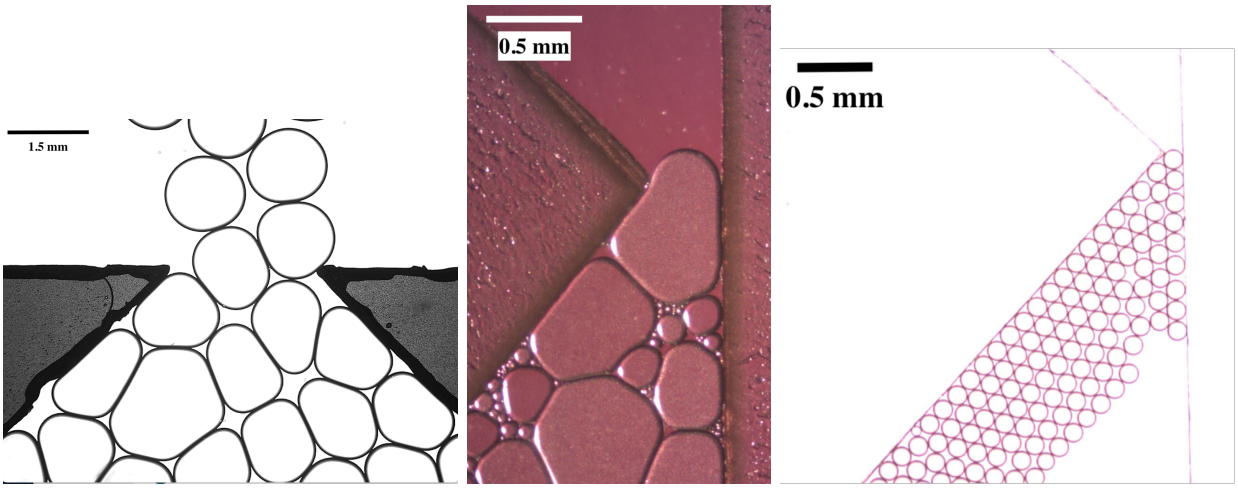

Figure 2.1: Images of oil moving through hopper. The left and right images are silicon oil-in-water emulsions produced through the use of a microfluidic device. The center image is a vegetable oil-in-water emulsion produced from shaking a bottle. The hopper materials vary, left to right, from laser cut plastic, to double sided sticky tape to glass coverslips. The sizes and polydispersities vary drastically between images. The right image has a polydispersity of $\delta \sim 20\%$, the middle image has a polydispersity above $\delta \sim 70\%$, and the right image has a polydispersity around $\delta \sim 5\%$

showing oil droplets, but some more flexible than others.

While shaking a bottle mixed with oil and water produces an emulsion, hopper experiments traditionally work with a narrow range of diameters measured by the term polydispersity, which is defined as the ratio between the standard deviation of diameter to the average diameter; $\delta = \frac{\sqrt{\langle \Delta R^2 \rangle}}{\langle R \rangle}$. The right image in Fig.2.1, for instance, has a low polydispersity, whereas the central image, which used "shaken bottle" emulsions, has a high polydispersity. For this project, I need to produce droplets with a polydispersity between $\delta = 5\% \rightarrow 15\%$ in accordance with prior experimental and computational work. The higher limit is so that we do not have small particles which can traverse 3-dimensional space, since these small particles can dart around the chamber. Conversely, small polydispersity throws out large particles, which take up a significant area of droplet coverage, but only count as 1 droplet. There are other reasons as well to a mix of large and small droplets, but the rationale requires that we first examine what our set up looks like.

Surfactant

Droplet coalescence is an issue for my experiment because it increases the polydispersity and reduces the overall number of droplets. Moreover, what will I do if two droplets become one in the middle of shooting a movie? Most critical in this respect is that coalescence increases in likelihood according to the external pressure of the droplets. Hence, the most likely place of coalescence is right at the hopper exit— this will not do.

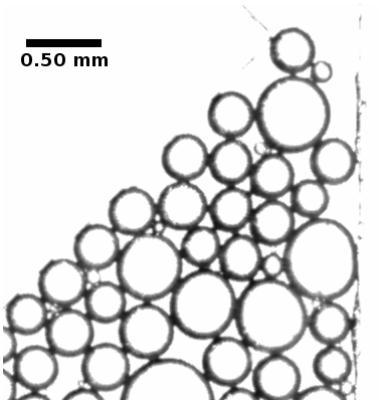

Figure 2.2: Image demonstrating the danger of too much surfactant. The droplets in this image clog the opening, despite the open space.

To aid in the stabilisation of emulsions, I use a 5% Tween 20 surfactant solution [22]. A surfactant stabilises the droplets because it consists of a hydrophobic tail and a hydrophilic head. The surfactant will coat the droplets such that the tail will point towards the oil and the head towards the water. This means that two droplets in contact with each other will have a thin double layer of hydrophilic heads which repel each other, preventing coalescence.

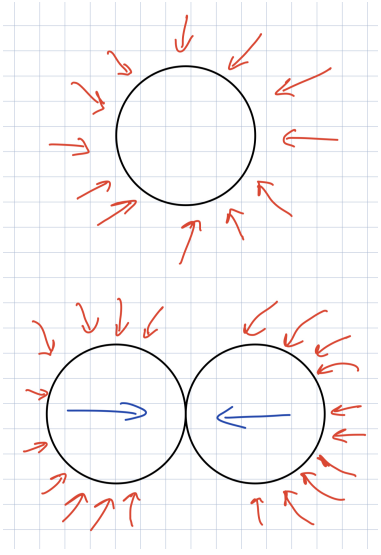

Figure 2.3: Image demonstrating depletion effect. Pressure imbalance causes droplets to "stick" together.

One brief note is that we find the surfactant is needed for generating *any* kind of flow. For instance, I create some chambers that have no surfactant, i.e. purely water and oil, and find that the droplets "stick" to the floor and ceiling microscope slides. This suggests that the surfactant is helping lubricate the glass surface, allowing droplets to the flow. Even at no risk of coalescence, for instance in our trials of one large droplet, surfactant is necessary.

But, too much surfactant produces globs of surfactant called micelles. Micelles occur when the concentration of surfactant is high enough such that the surfactant finds it energetically favorable to create a ball whose surface is made of hydrophilic heads and whose interior is filled with hydrophobic tails. This

configuration excludes water from entering the micelle, thus satisfying the hydrophobic tail. But, the presence of these micelles introduces what is known as a depletion force.

To understand the depletion force, imagine these micelles as small hard balls that are bouncing around in a liquid with oil droplets. The movement of the micelles is entirely random, so that when they hit a stationary oil droplet, the probability of these collisions is uniform around the edge of the droplet, as shown in Fig.2.3. If these collisions were not random, then our droplet would magically start moving. We say that these collisions are isotropic. When two droplets are close together, as we see in the bottom section of Fig.2.3, the micelles cannot collide with the droplets from the inside, leading to a pressure imbalance that keeps the droplets "stuck" together. This stickiness is called the depletion force, and its effect is shown in Fig.2.2. As such, we should be careful not to inject too much surfactant, so as to avoid the production of micelles.

2.1.1 Snap Off Through Direct Syringe Injection

A method for generating droplets within my desired range of polydispersity is called the snap off method, taken from Barkley *et al* [2]. There, Barkley slowly flows oil through a small glass syringe, as seen in Fig.2.4. Once a critical radius is reached, the buoyancy of the droplet snaps the droplet off the tip. Barkley concludes that the inner diameter of the syringe determines the characteristic size of droplets, producing droplets with an overall polydispersity less than $\delta < 1\%$. I use this technique for the production of droplets in my experiment.

To set the size of the needle's inner diameter, I use a Sutter Instruments Model P-97 Flaming Brown Micropipette Puller and a Narishige MF-830 Micro Forge. The micropipette puller heats the glass pipette and pulls it apart, creating two needles. The result is the same as when a putty is pulled from two sides, creating a thin elongated stream where the break occurs. I then place one of syringes in the micro forge, where a hot knife cuts off the excess glass. The micro forge is encased within a microscope equipped with a fitted ruler. This

allows me to cut the glass to the specified inner diameter.

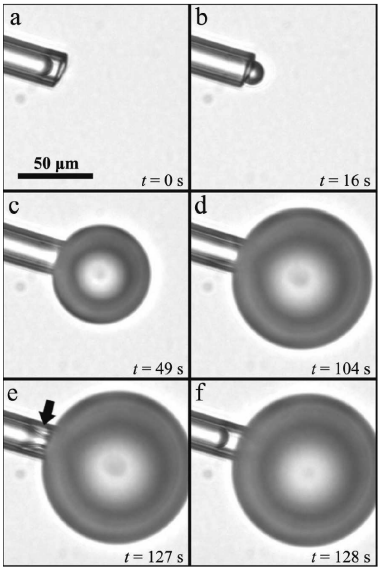

Figure 2.4: Snap-off procedure for droplet creation. Slow injection of oil allows droplets to snap off at a critical size given by the inner diameter of the needle. Taken from Barkley *et al.* [2].

I then glue this glass needle to a Luer lock syringe tip, lock this onto a syringe barrel and place the syringe on a syringe pump. The specifics of chamber design will come later, but for now, suffice it to say that a chamber is a box with an extremely small thickness ($d \approx 250\mu m$ between two $75 \times 50mm$ microscope slides). I find it easier to thread the needle in between these plates and directly inject oil into the chamber than creating the droplets in a separate container and transferring them. To help this process, I use a retooled microscope frame, shown in Fig.2.5 to help guide the needle with steadiness as I lower the needle into chamber, assuring that the fragile tip of the needle stays intact.

The flow rate I use is typically $f = 0.0001$ mlmin^{-1}— the fastest rate I find that sustains the required polydispersity and keeps the pressure from bursting the fragile glass needle. This slow flow condition means that a chamber can typically take an 1-2 hours to fill. As such, this method for making oil-in-water emulsions was used mainly for the one droplet chambers.

2.1.2 Microfluidic Device

Another method for droplet creation uses a microfluidic device. A microfluidic device uses two streams of fluid, a continuous phase and a dispersed phase, to create droplets. The device works by pumping the continuous phase at a higher velocity than the dispersed phase such that it tears or cuts away droplets of oil from the oil stream itself. Images taken from the production of droplets are shown in Fig.2.6. If the pressure is stable within the apparatus, then the droplets are created with moderately low polydispersities ($\delta = 5 - 10\%$), and, unlike the syringe injection, produced in the amount of tens per second. Hence, the microfluidic

device is excellent at producing a large number of droplets with low polydispersity— the ideal device for many droplet chambers.

In theory, the size of the droplets is determined by the relative rates of the continuous and dispersed phase [15, 19]. In my experiment, however, the desired size of droplets ($d \approx 315\mu m$) brushes up against the upward limit determined by the constraints of the device itself, viz. the inner diameter of the channels. This means that I drive the microfluidic device in an unsteady region where slight pressure changes can rapidly shift the characteristic size of droplets. This issue is only compounded by the use of syringe pumps which can produce pressure transients— as opposed to pressure pumps which maintain steady pressure by driving flow through the direct manipulation of pressure — given that pressure is only a knock on effect of the pump itself. That is to say, syringe pumps compress a plunger which in turn induces a pressure differential in the tubes to pump out the fluid— although the rate of this compression is relatively controlled (at smaller flow rates the motor "discretely" pump fluid in bursts) the pressure differential can be far from it. Ultimately, this causes a wide, undesirable range of droplet sizes; many with diameters smaller than the thickness of the plates, meaning that our condition of quasi-2d flow stands unmet.

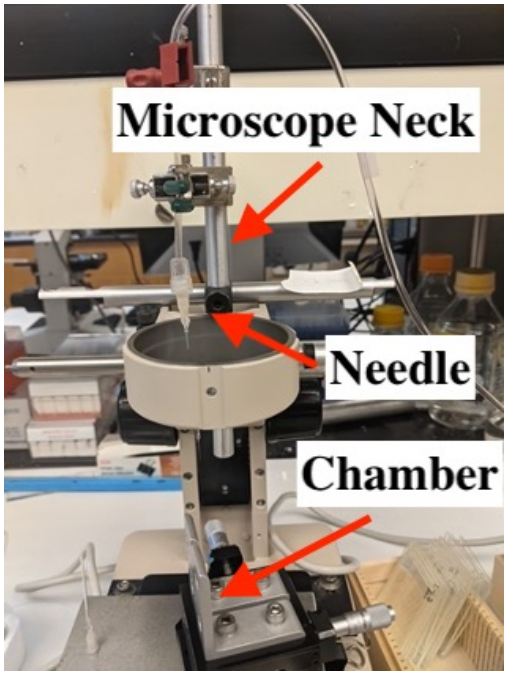

Figure 2.5: Image of the set used to inject oil into hoppers. The needle comes in from above and is anchored to a pole which can be moved up and down by the rotation of a knob. The bottom platform is also adjustable by two knobs that move translate the platform horizontally, allowing me to finely guide the needle into the chamber without snapping it.

To fix this, I first place the device under a microscope so that I can examine the types of droplets being produced. This allowed me to develop the ensuing strategy: first, I run the dispersed phase at a constant injection rate of 15mLmin^{-1} and the continuous phase at a rate of 40mLmin^{-1}. This creates a regime where both the continuous and dispersed phases

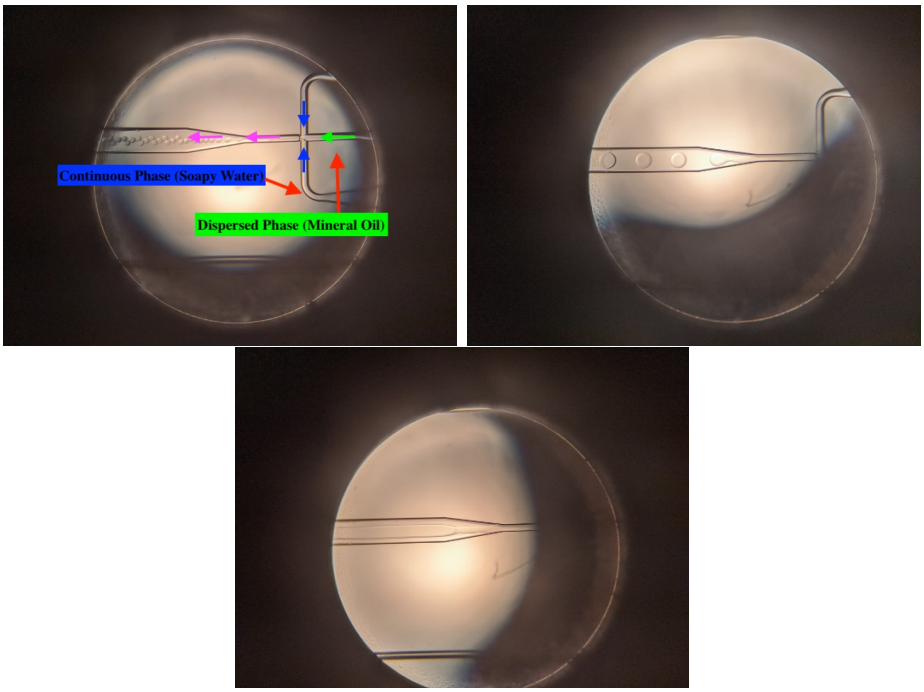

Figure 2.6: Images of three regions of microfluidic droplet production under a microscope. The bottom image is the starting image of stable co-flow region where oil and water flow without droplet creation. The top left is the region where droplets are pinched off by the continuous phase, but too small to be used in hopper experiments. The top right is the region I select droplets from, which are appropriately sized and polydisperse. For scale, the the width of the tubes is $425\mu m$.

"co-flow", as is seen with the two "bars" of fluid in Fig.2.6. If I do not achieve this regime at the start, then I pump the dispersed phase at a very high injection rate ($\approx 120\text{mLmin}^{-1}$) to let the dispersed phase break through. Once stable co-flow is achieved, I then switch off the dispersed phase syringe pump for roughly $5-10$ seconds. This has the effect of pulling the dispersed phase back, and letting the continuous phase "run ahead" by reducing the pressure of the dispersed phase's emergence. After a couple rounds of turning off the syringe pump, I achieve the state seen in top left of Fig.2.6. To maintain this state, I visually track the trend in droplet sizes: if they are increasing in size then I turn the dispersed phase off to let the continuous get an edge; if the droplets are decreasing in size, I turn the continuous phase off to give the dispersed phase a chance.

2.2 Chamber Design

A chamber denotes a box with a very thin width where I place my oil droplets to flow. A chamber consists of a hopper sealed between two plates. The chambers themselves are made from two 75×50 mm microscope slides. I place the hopper inside the chamber to add volume to the chamber, and glue the chamber shut with Optical Adhesive #68. In the course of this project, I have used different hopper designs and production techniques.

2.2.1 Hopper Material

The first batch of chambers I used to explore the important features of this project, before gathering any data, was a reproduction of the chamber design used in Hofert [12]. This hopper design cut out double sided sticky tape, pasted it to a slide and sealed the slide with an ultraviolet drying adhesive Norland UV epoxy #68. Per Hofert , I use two layers of sticky tape stuck to each other in order to increase the thickness of the chamber [12]. This creates a chamber of roughly $d \approx 300\mu m$. Because these chambers were used to explore the workings of the microscope and lighting stages, meaning that the emulsions in these chambers were "shaken production" with high polydispersities, the thickness of the chamber was not calibrated in the manner of later designs to create quasi-2d systems.

While these tape chambers were indispensable for understanding the important control knobs for microscopy (to be discussed later), they ultimately proved to be too uncontrollable for experimental results. Namely, because the double layer of tape could not be accurately aligned, there were often staggers introduced at the edges, creating "shelves" which could pin droplets— an effect amplified by the stickiness of the tape itself. Along this same theme of alignment, the relative angle of the hopper was difficult to control, even with the use of an alignment tool, since the tape left a residue on the slide if lifted and moved. Moreover, left over time, a reside would begin to form, most likely from soaking sticky tape in a liquid, which would limit the reusability of the chambers after one hour in some cases.

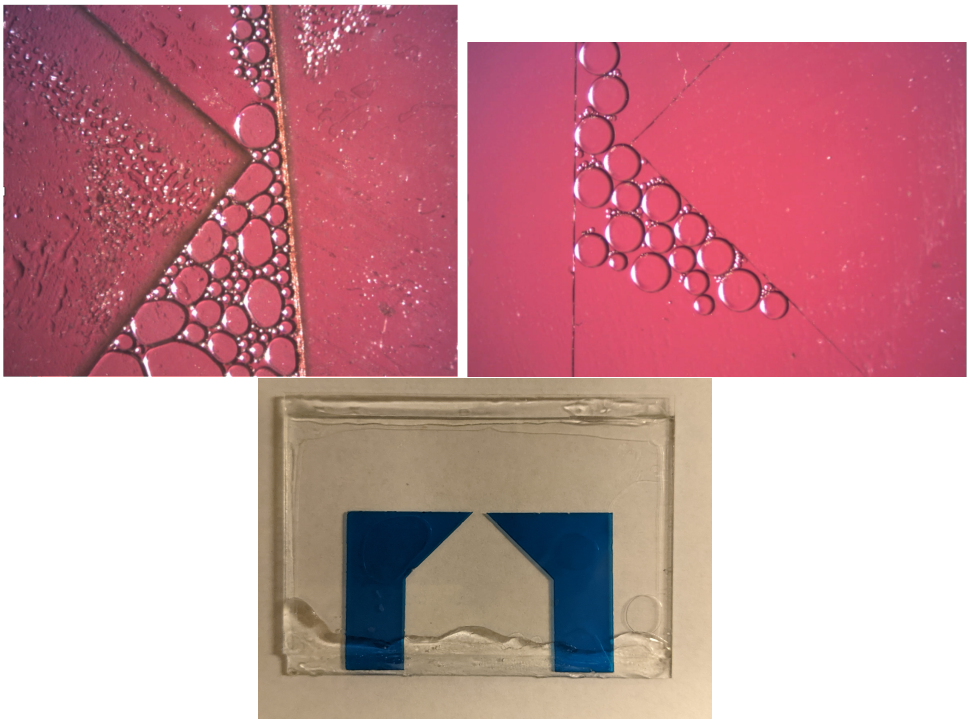

Figure 2.7: Images of three different chambers. Top left is double sided sticky tape with shaken bottle emulsions. Top right is glass coverslips with snap off emulsions. For scale on top images, the opening is roughly $\sim 500\mu m$. Bottom is laser cut plastic with microfluidic emulsions. For the scale, the slide has dimensions of $75 \times 50mm$.

The next hopper material I used were size 2 glass coverslips, as seen on the right in Fig.2.7. Because the coverslips are not coated with any sticking substance, I placed a small drop of Norland UV epoxy #81. This glue also dries under ultraviolet light, but is much less viscous and dries in seconds as opposed to the 3-4 minute time of #68. By adding a small drop of glue to the coverslips, the overall thickness of the chamber increases slightly. Moreover, a slight gap is introduced between the lab slide and the coverslip. I try to minimise this gap by pressing the coverslip into the microscope slide, but when filling the chambers, I noticed that the surfactant solution would get in this gap. However, because the oil droplets have higher surface tensions, which makes it difficult to deform into less spherical shapes, the oil droplets never get pinned, always flowing along the edge of the slip. These coverslips fixed the residue problems of the tape, allowing me to reuse chambers.

A brief, but small issue with coverslips is the manufacturers error on the coverslip thickness which can range along $\delta \approx 0.04\mu m$ (which could has also been true for the tape but given that

I was only testing loose protocols with the tape chambers, this slight detail missed my eye). What is concerning about this difference is that the two microscope slides will no longer be parallel to one another. Because the surface tension pushes the bubbles toward the direction that will maximise their spherical shape, the imbalance of plates results in a preferred side that the bubbles will drift to. To counter this, I use a micrometer to measure the thickness and ensure that the two coverslips I match up do not blatantly outsize one another.

The larger issue with the coverslips is that the shape and size of the slips are themselves immutable. And the given square shape does not lend itself to corralling the droplets, meaning that many droplets do not pass through the hopper, but flow along the outside edge. To fix this, I use plastic sheets that I laser cut into experimentally useful shapes. To determine this shape, I look to Hofert, Tao *et al.* and Hong *et al.* for inspiration [12, 18, 13]. Ultimately, I settle on the shape given in Fig.2.7.

Looking to the derivation of Eq.3.1, we find that the difference between the asymmetric and symmetric hopper openings will not play a role. A fortiori, an asymmetric hopper with the same number of droplets as a symmetric hopper *will* exert more pressure on the exiting droplets since the droplets are stacked higher, thus increasing the flow rate— but the symmetric hopper doubles the effective opening width of the asymmetric hopper, which *also* increases the flow rate.

These laser cut hoppers are the best evolution of the hopper design for multiple reasons. They have the chemical inertness of the glass coverslips that makes them reusable. They are, in fact, easier to align than the glass coverslips since the flat base can be set using a straight edge that simultaneously aligns the hopper angle as well as the angle relative to gravity. Moreover, since the pieces are cut from the same sheet of plastic, the error in thickness is much smaller. That said, they are not adhesive in any way, so they do require spot bonding. Looking at Fig.2.7, I spot bond the top of the "boot" which juts out of the chamber anyway. As such, gluing at this location minimises the unwanted thickness of the glue.

This hopper design is shown in the bottom of Fig.2.7. Under a microscope, this hopper is

shown on the right in Fig.3.5.

2.2.2 Hopper Initialization

To match the initial static state of simulated hopper flow, a large air or oil bubble was introduced to clog the opening, letting the droplets stack against it and build hydrostatic pressure as seen in Fig.2.8. The large air-bubble was then squeezed through by gyration or pressing against the chamber. We find that this bubble effectively reproduces the unplugging phenomenon from prior work, by helping meet the pressure conditions required for the application of Eq.3.1.

Prior to this method, droplets could only build the requisite pressure after a large portion had already passed through, which is to say that this method not only matches the traditional hopper initialisation setting, but also increases the amount of useable data by extending the amount of droplets that are part of the hopper flow.

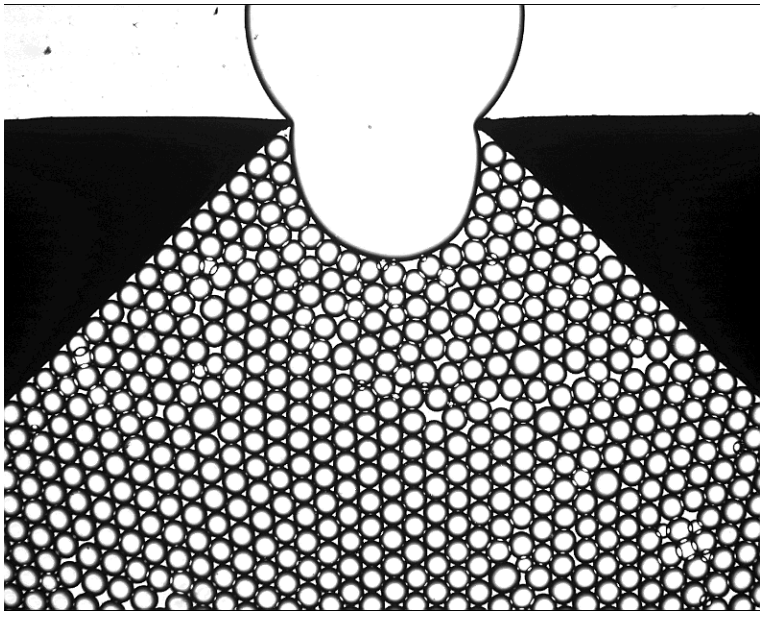

Figure 2.8: Image taken of large droplet deliberately produced to clog opening. This allows droplets to stack behind, recreating the initial "plugged" conditions in simulations. The large droplet is squeezed out by pressing against the glass with light pressure. For scale, the opening width is $w = 2.2mm$.

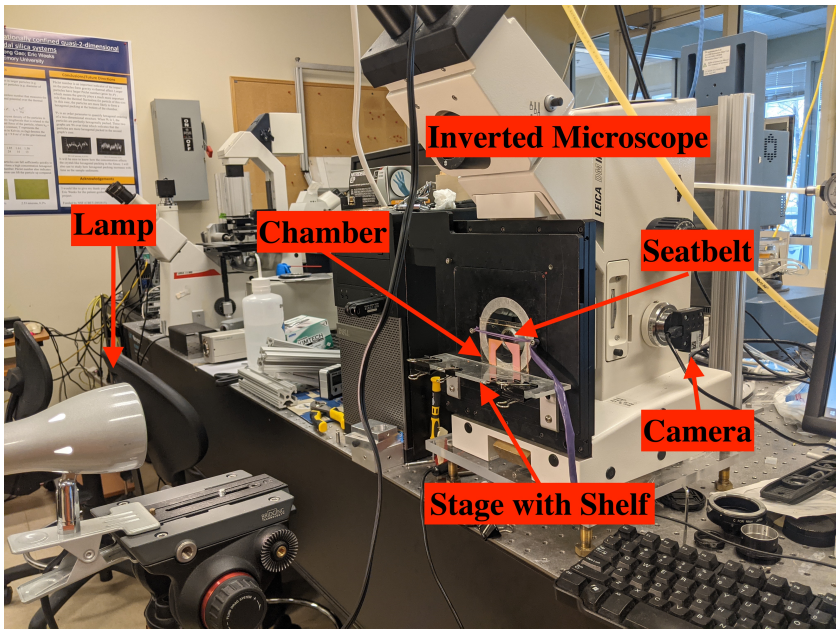

Figure 2.9: Image of imaging apparatus, with a rotated microscope, light source on tripod, a chamber fastened by its seat-belt, resting on a shelf that juts out from the stage.

2.3 Microscopy

An inverted Leica DM IRB microscope, outfitted with a ThorLabs DCC1545M CMOS camera is used to image and record the droplets at 4 frames per second. In all trials, the microscope is fitted with a 1.6× lens and the camera is mounted with a 0.35× C mount. Together, the lens and the C mount give me a sufficiently large field of view to allow a glimpse at the dynamics of particles far from the opening without losing the resolution necessary for imaging and distinguishing droplets from one another. After calibration, I find that 151 pixels is equal to 1 mm. The set up is shown in Fig.2.9.

Because the inverted microscope we use is rotated to align the stage with the direction of gravity, as shown in Fig.2.9, I was forced to remove the arm on the microscope that lights up the stage. To remedy this, I combine a common desk lamp with a variable height camera stand. This apparatus gives me a large amount of room to play with the lighting. In particular, this lighting set up allows me to control and root out the shadows cast on the droplets. This is especially useful since our tracking algorithm detects and measures droplets by looking for connected regions of white pixels. If there is an asymmetric shadow cast on the

image, or glare, the algorithm will miscalculate the deformation or, worse, miss the droplet altogether.

Another issue in rotating the microscope stage is getting the chamber to stay in place. Early on, I use the method described in Hofert of taping the chamber to the stage [12]. This method, however, produces extremely variable results, since the chamber can be rotated off the direction of gravity. To fix this, I use a different microscope stage that has threaded holes. This allows me to create a "shelf" on the stage with two metal brackets and a sheet of acrylic. To keep the chamber pressed against the stage I take advantage of two other holes on the stage to create a "seat belt" out of a rubber belt. Together, the seat belt and shelf allow me to easily align my chambers with gravity.

2.4 Computational Work

2.4.1 Particle Tracking

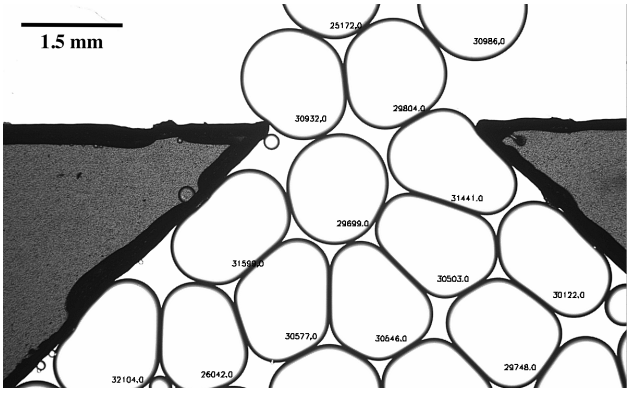

Figure 2.10: Image taken from lblmovie.pro. The numbers inside the droplets give the area in pixels corresponding to that droplet, but the function could print whatever property is desired.

To identify and track droplets, I use software developed by Crocker, Grier and Weeks [8, 9]. The software uses identifies regions of connected white pixels in a pre-tracking phase and then connects these regions through a tracking algorithm that finds the nearest white region between frames. In addition, this software also calculates many useful physical properties of the droplets, such as the area, perimeter, deformation and others.

Because, however, the gaps between droplets often count as closed white regions, the software requires a careful set of criteria to discriminate between droplets and gaps.

To help this process, I develop a couple algorithms to identify what these criteria should

be. Since the software works in pixels, it can be difficult to imagine what an area of 300 square pixels looks like. For this reason, I wrote a program called lblmovie.pro which plays the movie and prints the desired property for each droplet inside the droplet, as shown in Fig.2.10. This gives me a more intuitive understanding these properties. I then identify the range that the droplets fit in and cut out the rest.

Often times, however, the properties of a gap will fit within the criteria of droplets, meaning that removing the gap means removal of the droplets. For this reason, I also write a procedure that I allows me to click on the image to remove a white region from the tracking data.

2.4.2 Measuring Flux

To measure the flux, I write a program that counts the number of droplets that pass the y position of the hopper between two frames (0.25 seconds) and multiplies each droplet by its particular area divided by the average area of droplets. I then smooth over the data through a boxcar average that takes the average of number of droplets exiting over a specified length. I generally smooth the data over a $2.5 \rightarrow 3.0$ second range, meaning that the recorded flux at a time t is really the average flux over the range of $t - 3 \rightarrow t + 3$. While smoothing helps get rid of the intermediate regions where IDL records no flow, overuse can wash out and suppress the slope of the curve, since smoothing tends to level the data. For this reason, I smooth the data over a window size of at most ~ 4 seconds.

Chapter 3

Multiple Particle Results and Analysis

Using the outlined techniques, I record 41 movies suitable for tracking and the extraction of hopper flow data. While we are poised from this collection to address the specific problem of hopper flow, i.e. the determination of β for soft, frictionless flow, the overarching goal remains to characterise features of hopper flow for soft frictionless droplets in general. Let us begin by examining the basic element we can surmise from our tracking algorithm— the trajectory of droplets.

3.1 Trajectory of Droplets

Peripherally, looking at Fig.3.1, we immediately encounter an interesting phenomenon— the trajectory of droplets appears to become more discretised for droplets more closely aligned with the wall. That is to say, we see defined lines of allowed flow followed by gaps that are emptied, for the most part, of trajectories. Occasionally, we see a trajectory that crosses these badlands, and these transgressing trajectories line up with the direction of gravity and, by extension,

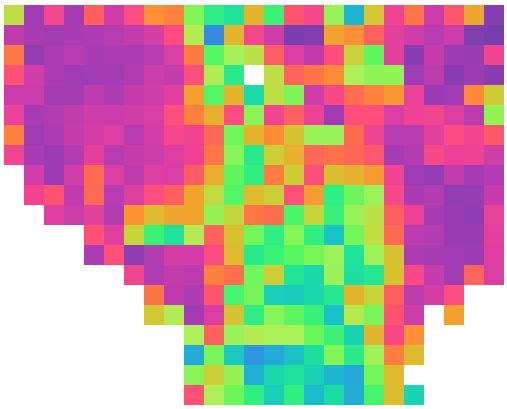

Figure 3.2: Contour plot for ψ_6. Purple represents $\psi_6 = 1$ and blue represents a $\psi_6 = 0$.

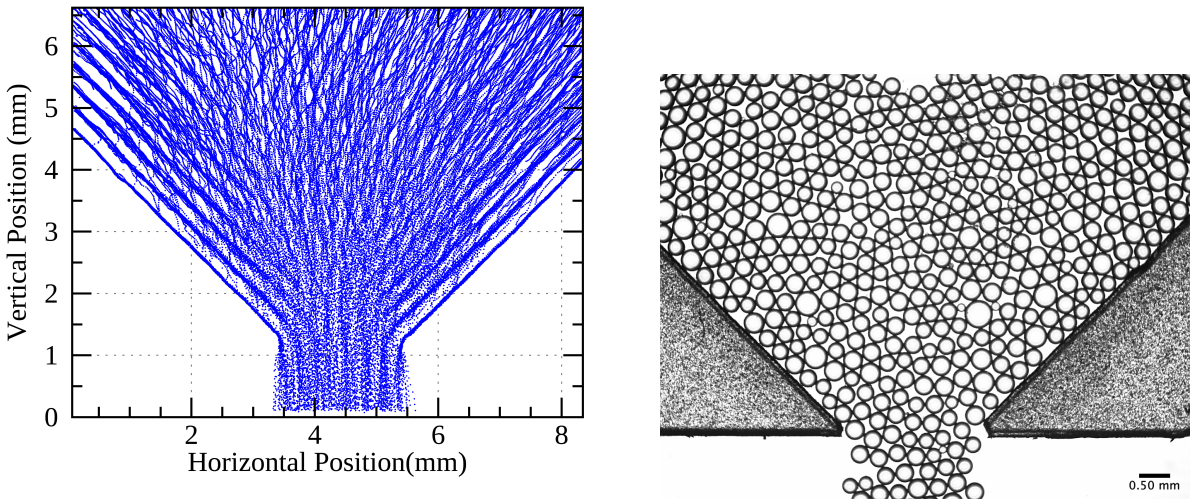

Figure 3.1: Still image from hopper flow and trajectory of droplets over a 25 second range. Each line represents the trajectory of a droplet navigating through the hopper. In this trial $w/d = 7.4$, with $d \sim 304$ at a polydispersity of $\delta = 8\%$.

the direction of droplet flow.

I roughly calculate the distance between the first and second order lines and find that they correspond the the diameter of the droplets. This suggests that the trajectories along the wall are the trajectories that correspond to a "unit" of crystalline droplets travelling with a group flow. This suggests that gaps in between are features of the way that droplets are located at integer steps within a crystalline structure.

We can test wall crystallinity by looking at a parameter called ψ_6. This parameter measures the angles between neighboring droplets in order to calculate how hexagonally packed these neighbors are. If they are hexagonally packed, then the droplets are located at equidistant angles of $\pi/6$ from each other, and $\psi_6 = 1$. Any deviation means that there is not as strong hexagonal ordering and ψ_6 will subsequently dip. In Fig.3.2 I create a contour plot that that assigns a value of ψ_6 for each x and y point in the hopper over a small period of time (~ 3 seconds). There, we see that crystalline structures are present near the walls, as we predicted, and this crystallinity disappears for the droplets over the exiting beam.

The interesting results from this suggest that crystallinity occurs from two distinct phenomena: 1) the pressure of droplets being pushed against the wall 2) the difficulty for

droplets along the wall to exit. That is to say, if we compress a pile of shaving cream with our hand, the shaving cream will spread out laterally. This compression mimics the effect of pressure 1). What these crystalline structures tell us, however, is that we have another pressure that keeps the droplets compact, not allowing them to spread laterally like our pile of shaving cream. This latter idea suggests an important interaction between flow and the exit itself. Let us examine this more closely by tracking the velocity profiles of the droplets.

3.2 Velocity Profiles

For a general understanding, I plot a heat map for the speed of droplets as a function of location in the hopper, given in Fig.3.3. There, we see three trends: 1) Droplets move faster the closer they are to the exit 2) Droplets along the walls tend to move slower than droplets in the center 3) The droplets pressed against the walls, but near the exit, have a wide range of speeds, from very slow to very fast.

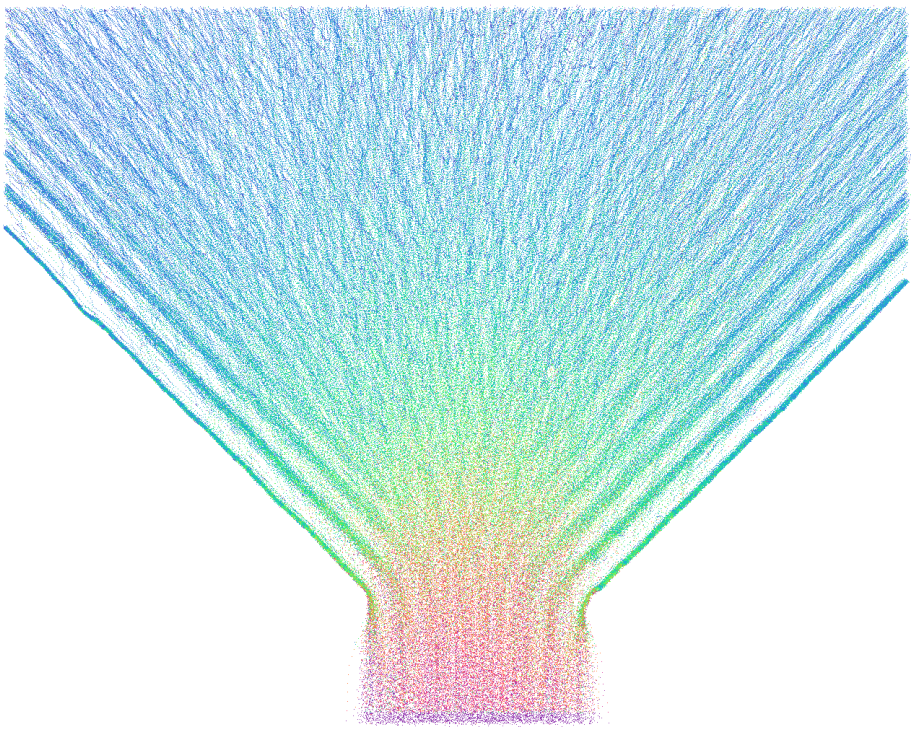

Figure 3.3: A heat map representing the speed of droplets flowing through a hopper. Blue represents the slowest speed to through red to purple which represents the fastest. $w/d = 7.4$ for this experiment.

The first two behaviours are better understood when we break the heat map into slices, shown in Fig.3.4. The bottom graph shows that the vertical velocity of droplets as a function of vertical distance from the hopper increases until the droplets are close to the exit, upon which their vertical velocity levels out to terminal velocity. Around $y = 1.5mm$, where the exit is, there is a small dip in the average vertical velocities. This suggests a crucial droplet wall interaction. Droplets near the exit, but on the wall, are given second priority to depart relative to droplets directly within the vertical beam of the hopper. As such, these droplets are made to wait until an opening occurs, whereupon the droplet can enter the exit beam. Because these droplets were stationary their velocity accelerates from $v = 0$, hence the dip in vertical velocities near the exit.

This waiting behavior can be further evinced when we look at the vertical and horizontal velocities as a function of horizontal position, graphed in Fig.3.4. The different colors correspond to slices of different heights above the exit, from navy blue which represents the region from the hopper exit to $0.75mm$ above the exit, to gold which is $4mm$ to $4.75mm$ above the exit. From the horizontal velocity graph, we see that droplets near the walls move with greater non-affine motion to the direction of gravity than droplets in the center— as we expect given that the normal force of the walls repel droplets perpendicular relative to themselves, but 45° relative to gravity. Interestingly, we see that the non-affine motion of droplets for the slice nearest the wall is not the greatest at the wall itself, but increases linearly until the region directly above the exit. This occurs because a droplet which is next in line cannot go any farther upward unless it moves off the wall. But, glancing at the vertical velocity for the slice nearest the exit, entering the exiting beam is no easy feat, since this beam is moving at a high velocity relative to the droplets on the wall.

This isolates the third phenomenon we see from the heat map. For, along the pincers, we have a mix of fast and slow moving droplets. That we simultaneously have droplets in waiting and fast moving droplets demonstrates that the droplets along the pincers are “eager” to exit. We can understand this by saying that droplets at the pincer are subjected to two

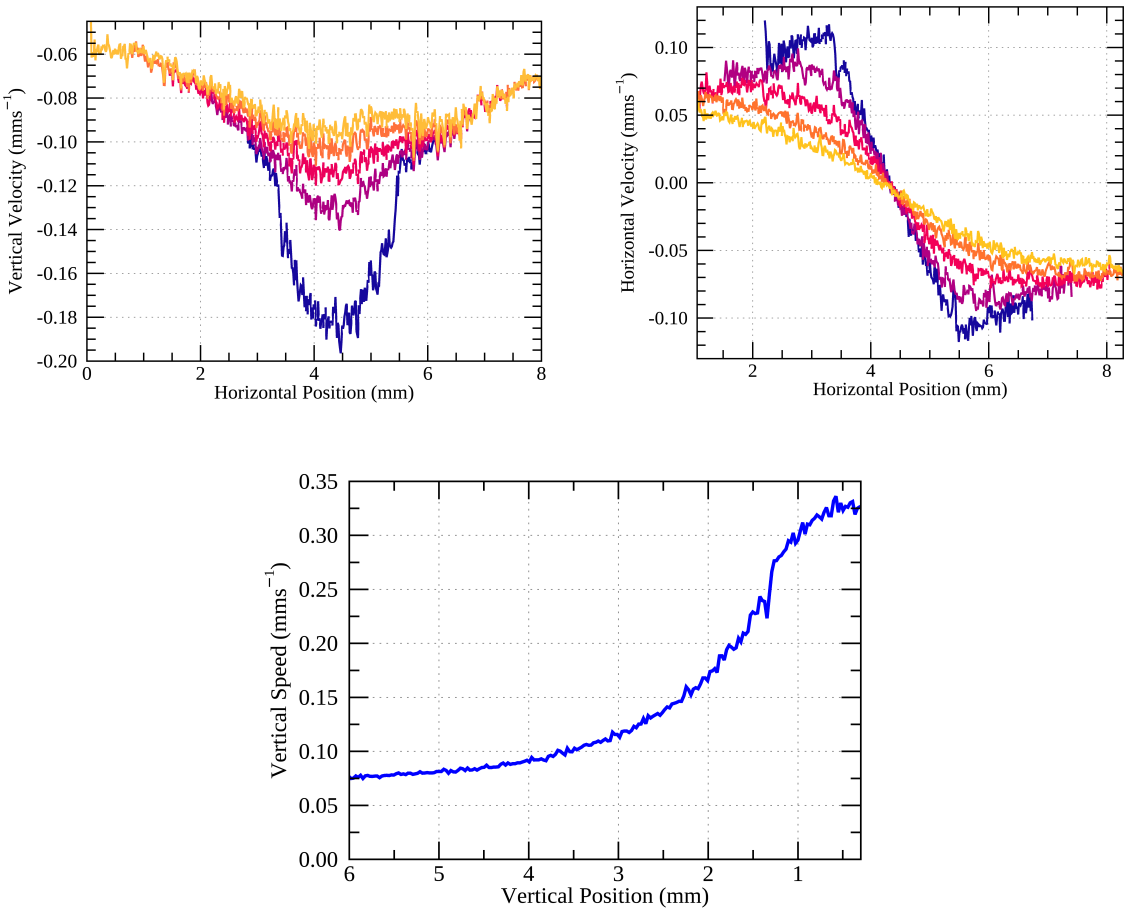

Figure 3.4: Velocity profiles of droplets filing through hopper. The top left and right graphs represent the vertical and horizontal velocities as a function of horizontal position. The different lines represent "slices" taken from regions of increasing height from the exit, where navy blue includes the hopper exit, to gold which is $\sim 4mm$ away from the hopper exit. For this trial, $w = 2.24mm$, $d = 304\mu m$ and $w/d = 7.4$. Note that then vertical speed is the negative of the vertical velocity. Also note that the hopper begins at $x_{left} = 3.3mm$ and ends at $x_{right} = 5.5mm$, aligning with the peaks on the purple curve of the top right graph.

strong, but equally matched sources of pressure: 1) the flow of droplets above the beam 2) the line of droplets behind the pincer. The first pushes the droplet back, while the latter pushes it forward. Once an opening appears for the tormented droplet, it not only falls into place; it is pushed there.

3.3 Flux

3.3.1 Flux for Soft Particles

If we are going to measure the flux of soft particles, we need a way to characterise flux for a system of soft particles. This is needed because soft particles, unlike hard ones, have a continuous pressure gradient. As such, the outflow dynamics of soft, buoyant particles is controlled by the exertion of pressure of the droplets attempting to lower their gravitational potential energy, alongside the negotiation of surface energy constraints that aim to keep the droplets circular [20]. Hence, as the oil flows out, this pressure steadily abates, corresponding to an equivalent decrease in hopper outflow.

With negligible friction, the outflow of particles goes as $\Delta\rho gh$, where $\Delta\rho$ is the difference in density between water and oil, g is the gravitational acceleration constant, and h is the height of oil above the hopper. That is, besides some constants, the flux of oil droplets is controlled by how many droplets are above loaded in the hopper, exerting pressure on the droplets near the orifice to exit. For a triangular hopper, shown in Fig.2.1, the height of droplets above the hopper squared goes, geometrically, as the area of droplet coverage. Assuming that each droplet occupies a relatively small portion of the overall area, then the hydrostatic pressure can be approximately written in terms of the number of droplets left. Hence, the flux:

$$\frac{dN}{dt} = c_0\sqrt{N}. \tag{3.1}$$

Where $\frac{dN}{dt}$ is the flow rate, N is the number of droplets loaded in the hopper, and c_0 is a proportionality constant. The question can now be posed: if we measure the flow rate as a function of $\sqrt{N}$, will the proportionality constant, c_0, fit to a power law? If so, what will its exponent be? That is to say, will the coefficients be fittable to the Beverloo equation:

$$c_0 = \mathrm{a}(w/d - \kappa)^{\beta}? \tag{3.2}$$

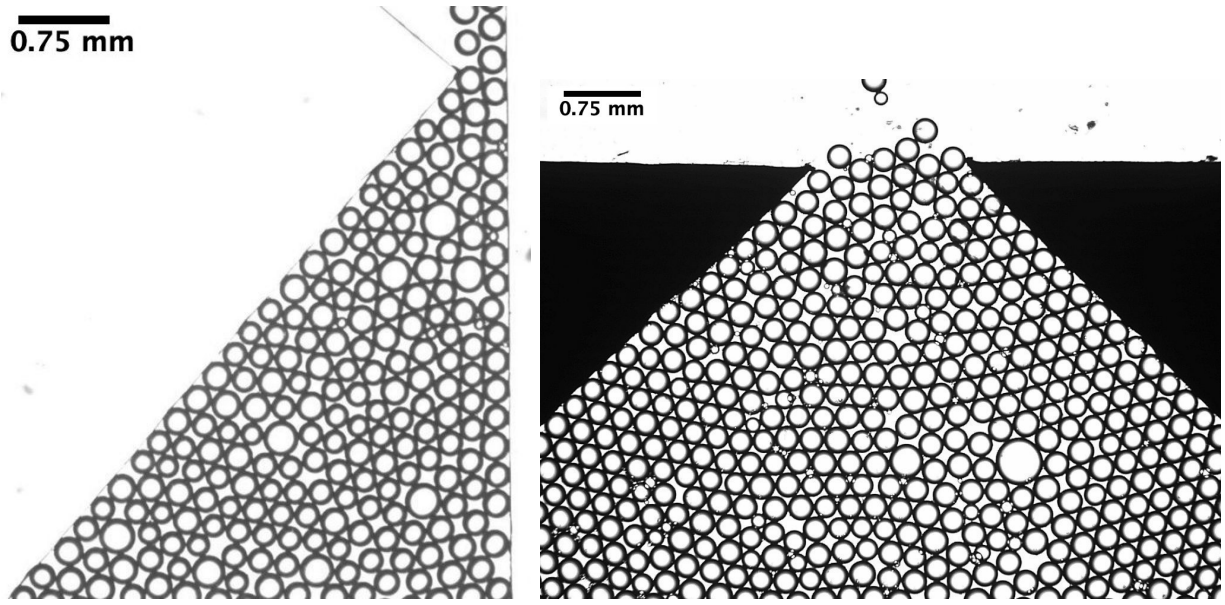

Figure 3.5: Two images of hopper flow under microscope. On the left, oil-in-water emulsions filing through glass hopper of opening size $490\mu m$ (thickness $\sim 210\mu m$) with $45°/90°$ walls. The average droplet has a diameter of $284\mu m$ with a 9% polydispersity and $w/d = 1.72$. On the right, oil-in-water emulsions filing through plastic hopper of opening size $2039\mu m$ (thickness $\sim 180\mu m$) with $45°/45°$ walls. The average droplet has a diameter of $298\mu m$ with a polydispersity of 7% and $w/d = 6.84$.

3.3.2 Experimental Data on Flux

I test Eq.3.1 by plotting $\frac{dN}{dt}$ against $\sqrt{N}$ in Fig.3.6. In Fig.3.6 we see a general trend that less droplets means slower flow, as we expect. That said, we also observe three regions of flow. We see an initial flow transient from $\sqrt{N} \approx 40$ on and a final flow transient from $\sqrt{N} \approx 14$ under. Between those two regions, we see a linear increase of flow rate as a function of $\sqrt{N}$.

The final and initial transients can be understood by examining the presumptions made in our derivation of Eq.3.1. One presumption of this derivation is the condition of requisite pressure. To understand, imagine that we have a hopper of 1200 particles and we release the particles one by one, so that they may file through. Clearly, our equation will break down since the particles are not exerting hydrostatic pressure on one another. On the other hand, imagine those same 1200 particles loaded in, ready to go, as shown in Fig.2.8. But, once this large oil bubble flows out, it drags the fluid with it, and by extension the surrounding droplets. As such, these droplets are being pulled by out a non-static field, which breaks with our derivation. Thus, these flow transients are features of the experiment which we can

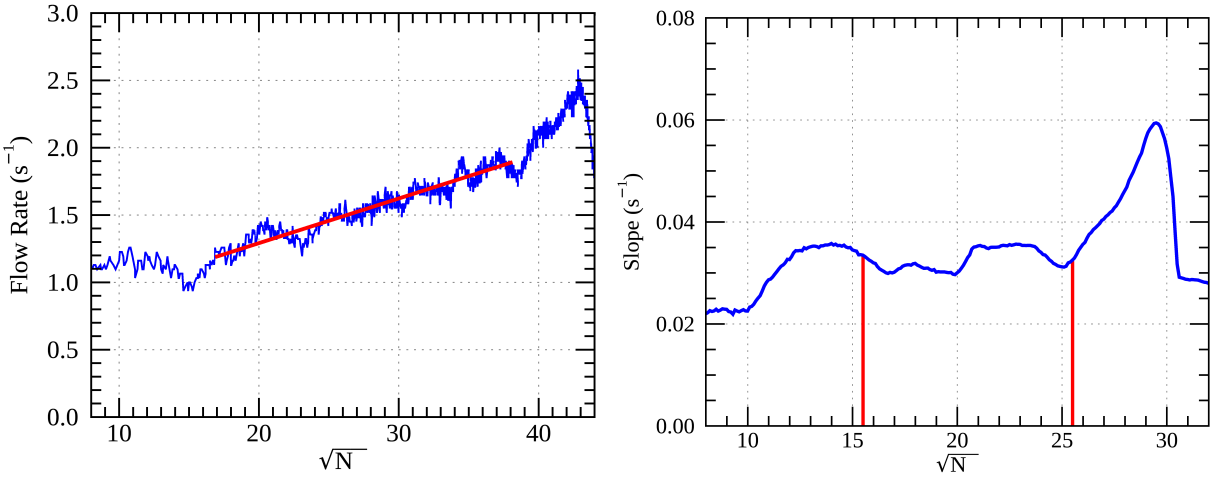

Figure 3.6: Graphs of flux as a function of the square root of remaining droplets and the Beverloo coefficients for a small range of fitting by means of ftfinder.pro. On the top, the number of droplets exiting as a function of the square root of how many droplets remain in the hopper, i.e. against decreasing time. On the bottom, the graph used to determine the appropriate region of fitting for the flux using ftfinder.pro. I look for flat regions on this graph to determine a steady region. The red lines on the bottom graph represent the desired flat region. The axes do not match since ftfinder.pro cuts off the indices which extend past the "ruler" length of the fit. For this case, the steady of region of flow ranges from $\sqrt{N} = 14 \rightarrow 24$. The red line on the top graph is fit to this established region of linear flow, following the equation $\frac{dN}{dt} = c_\circ\sqrt{N} + b_\circ$, with $c_\circ = 0.024s^{-1}$ and $b_\circ = 0.44s^{-1}$. The non-zero intercept is an artifact from omitting the initial and terminal droplets. For this trial, $w/d = 12.2$ and the average diameter was $305\mu m$.

account for, but must omit since they will not flow linearly.

Because of the final and initial pressure transients that break from the assumptions we make in in deriving Eq.3.1, the flux data will not match for the entire region of flow. For this reason, I write a function that helps me sort through the data, examining when the flow matches our conditions such that the parameter $c_\circ$ has meaning. First, I assume that the data has been linearised such that $\frac{dN}{dt}$ is plotted against $\sqrt{N}$. If this data is truly linear, then I should be able to slice a small range of the data,compare the slope to an adjacent slice and find no difference in value— where I measure the slope does not matter if the data is linear. For this reason, to determine the appropriate region of linear fitting necessary for determining $c_\circ$ from Eq.3.1, I measure the slop over a small range of the data (typically $\delta\sqrt{N} = 4 - 5$) and look for flat regions where the slope is approximately the same. Doing this generates a graph that shows me $c_\circ$ as a function of $\sqrt{N}$ for a small range of $\sqrt{N}$. This is shown as a companion to the flux data in Fig.3.6.

Overall, I find that trials strongly cohere to the principles laid out in Eq.3.1 for at least some range of $\sqrt{N}$— as seen in Fig.3.6 where the blue flux curve fits snugly on the red line. Moreover, I also find that the difference in hopper geometries does not change the $\sqrt{N}$ dependence.

As mentioned before, to determine the appropriate region of linear fitting, an IDL routine, ftfinder.pro, scans over the flux data and records the linear fitting parameters over partial regions of the data. Stable extrema of these parameters are taken to represent adequate zones of fitting. Typically, this tosses out the last (first in fig.3.6) 100 droplets. If the droplets have significant initial momentum then the first (last in fig.3.6) ~ 300 droplets are tossed out, but the initial clog of a large air bubble helps reduce the initial transient down to ~ 100 droplets. Intuitively, the tossed out regions correspond to the presence of unwanted initial pressure transients due to either the lack of hydrostatic pressure (when their was no forced initial clog) or the abundance of hydrostatic pressure (when droplets were gathered with a forced initial clog).

That said, I am occasionally forced to toss out certain trials for other reasons. This is mostly due to a poor tracking stage that misinterprets gaps and droplets, or to an error in droplet production that produces an untenable number of small ($< 30\mu m$ radius and therefore $<<$ thickness of the chamber) droplets. Some trials were well tracked, but tossed out because the linear region of fitting was over less than 20 droplets.

3.4 Fitting to the Beverloo Equation

Confirming that the flux of droplets goes as $\sqrt{N}$, I now move to the Beverloo equation that gathers these individual trials into a universal principle. What this means is that I take all those slopes from each trial and treat them as representatives of their individual w/d so that I can observe a general trend in how droplet flow relates to w/d. In Fig.3.7, then, I plot the slope, $c_\circ$, taken from Eq.3.1, against the ratio of opening width to average diameter, w/d, for

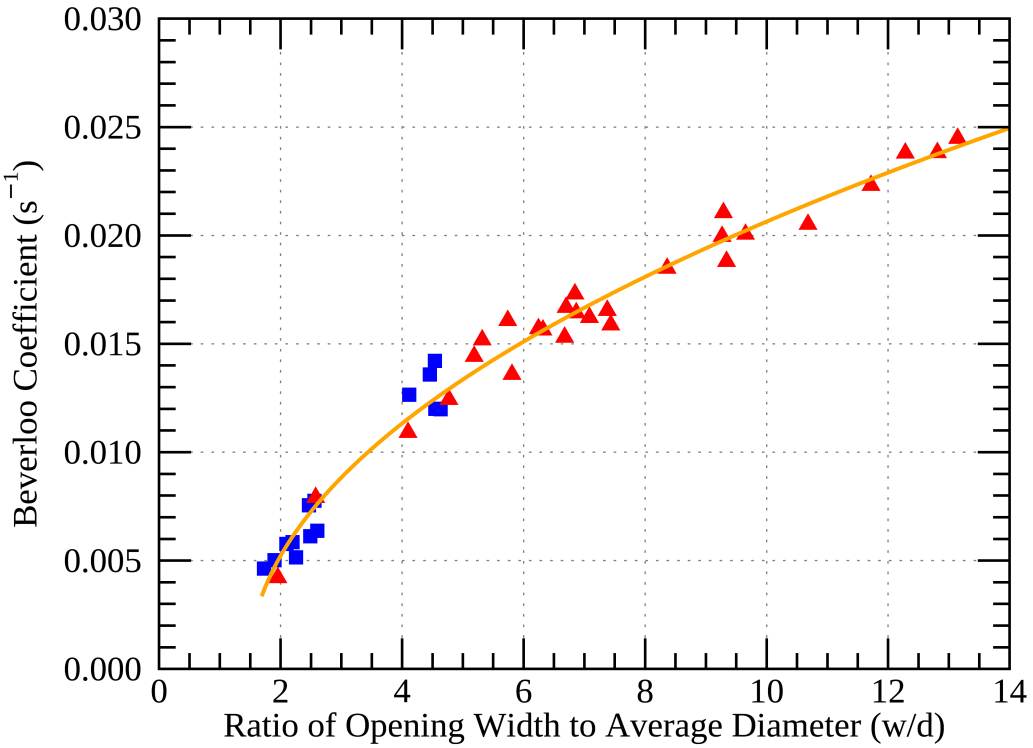

Figure 3.7: Power Law Fitting of Beverloo Coefficients. Coefficients of the flux mentioned in Eq.3.1, fitted to the equation $c_\circ = \mathrm{a}(w/d - \kappa)^\beta$, with a = 0.0071 s^{-1},$\kappa = 1.47$ $\beta = 0.49$. The blue squares were trials conducted with 45°/90° walls and red triangles were trials conducted with 45°/45° walls.

a range of $1.8 \leq w/d \leq 13.1$. There, we see that the data collapses to a fit, this fit is a power law, and its exponent is $\beta = 1/2$.

Again, we find an intuitive understanding of hopper flow at hand— if we increase the ratio of opening width to average diameter, the linear slope for our flux graph gets steeper. That is to say, we make it easier for droplets to depart from the hopper, because they can more readily take on an exiting posture without the need of hydrostatic pressure in the form of large N.

What is interesting, however, is that this pay off in flow rate levels out— increasing w/d starts to mean less and less for the flow rate. This idea is formalised when we fit these coefficients, achieving an exponent of $\beta = 1/2$. This tells us that we always get *some* payoff when we increase w/d but that it lessens the greater w/d was to begin with.

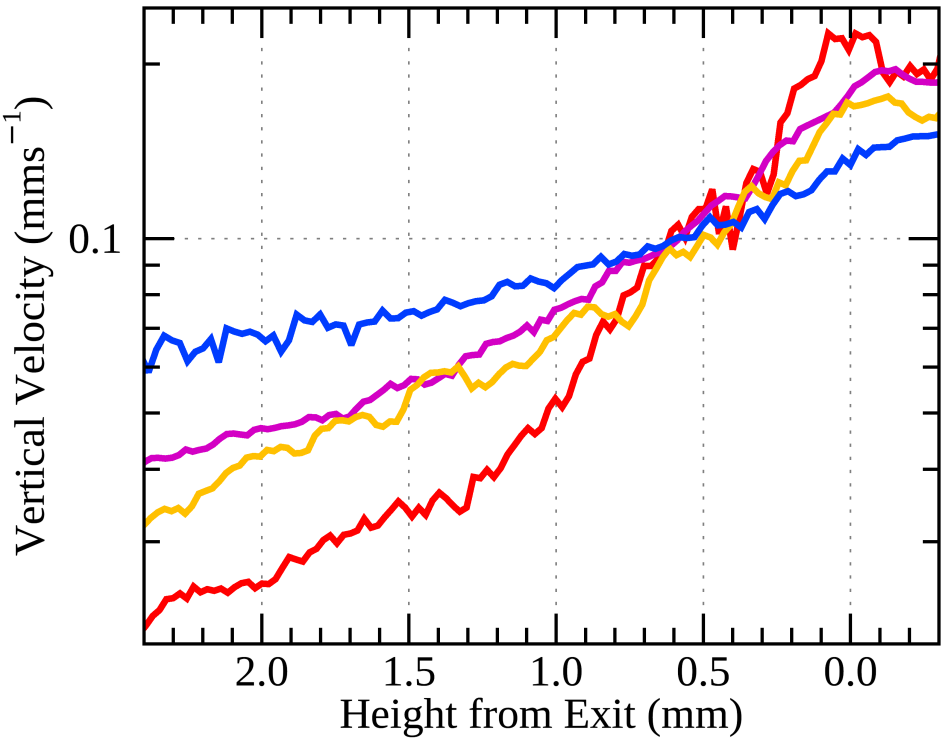

Figure 3.8: Graph of the average vertical velocity of droplets against the height, in pixels, for a range of w/d. The colors transition from red to blue as w/d increases, starting with $w/d = 2.1$ for red to $w/d = 4.5$ for blue.

This result becomes more interesting when we place it in the context of computational models discussed in the introduction— if the domination of viscous drag forces over kinetic friction, as we have recreated here, accounts for this exponent, then it should also account for this qualitative change in flow rate. After all, in the opposite limit, where kinetic friction dominates and $\beta = 3/2$, the pay off only keeps increasing as we move to greater and greater w/d.

If we follow the heuristic argument for the dependence of flux on dimension laid out in the introduction, we would expect for this characteristic frictionless payoff to manifest in the velocity profiles as a function of w/d. And we do indeed notice a trend in the vertical velocities, shown in Fig.3.8. On a global scale, the velocity of droplets levels out for larger w/d such that the difference in velocity between the droplets at the exit and the droplets far from the exit are moving at similar speeds. This flattening demonstrates the prominence

of viscous dissipation in our system, where Stokes' drag caps the velocity of the droplets, slowly approaching the scenario of droplets flowing down a hallway for larger w/d. So, as w/d increases, you can fit more droplets in, but the actual velocity of these exiting droplets decreases. Conversely, for smaller w/d we see that the velocity of droplets is *faster* at the exit than terminal velocity. So, we have less droplets, yes, but their velocities are faster than droplets for a larger w/d. Gathering these ideas together, when w/d is small, the number of droplets capable of exiting at once is also small, but their velocities are *larger* than the velocity of droplets in a larger w/d. The physical idea here is that smaller w/d means that droplets are being *ejected* from the hopper, and this ejection phenomenon decreases as w/d is increased. The decreasing payoff is a feature of the way that increasing w/d allows more droplets to flow through at once, thus increasing flow, but this increase simultaneously abates the ejection effect such that droplets are moving with slower velocities at the exit.

3.5 Summary of Findings

I have studied the dynamics of hopper flow for many particles with diameters smaller than the opening width. I have shown how the motion of droplets is affected by their location within the hopper, showing the presence of crystalline structures near the walls, and correlated this motion to the exiting beam directly over the orifice. Furthermore, I studied the flux of these soft, frictionless droplets, confirming the importance of hydrostatic pressure as the driver of particle flow. Finally, I have shown how this rate depends on w/d, and correlated this dependence to a power law with an exponent $\beta = 1/2$. This power law was explained through the velocity profiles for varying w/d, which suggested a trade off between number of droplets exiting and their velocity.

Chapter 4

Single Particle Results and Analysis

While the work on many particle flow was important for situating soft, frictionless particle flow within prior work on hopper flow, tracking the dynamics of one droplet can help us isolate and amplify the features necessary for the study of more deformable particles. As such, I now turn to my findings related to flow of one large ($d > w$) droplet. I am able to create 11 videos of droplets moving through the hopper. Each video contains $8 - 11$ trials of the same droplet moving through the hopper. I am occasionally forced to toss out a trial if the droplet does not initially strike the center of the chamber head on, but overall I find a remarkable level of consistency between trials.

4.1 Velocity

4.1.1 Durian Bubble Model

For this one droplet system, I focus on measuring and characterising the velocity of the droplet as a function of time, since the velocity can give us a an understanding of the forces acting on the droplet.

To get a sense for how prior work can help us think about this one droplet system, we can model a single droplet through recourse to the Durian bubble model. The Durian bubble

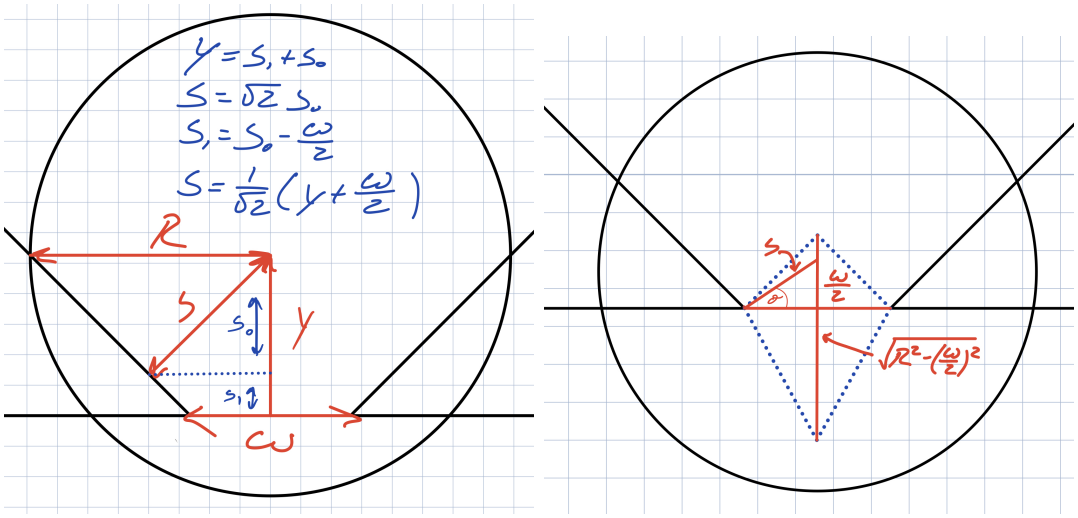

Figure 4.1: Geometry of single droplet flowing through hopper. R is the radius of the droplet, s is the distance from the center of the droplet to the wall, y is the distance from the center of the droplet to the center of the orifice, with $y = 0$ at the orifice itself, and θ is the angle between the center of the circle and the pincer of the hopper. The painted area is a diamond that begins from a height of $y = w/2$, when the center of the droplet can no longer form a perpendicular line to the wall. The painted region ends when the droplet has a position of $y < -\sqrt{R^2 - \left(\frac{w}{2}\right)^2}$. The left image corresponds to the region outside the paint. The right image corresponds to the region inside the paint. Note that the size of the paint varies with the size of the droplet, and the sketch proportions do not hold true generally.

model works by modelling droplets as circles which can overlap with each other and with walls. These overlaps are made to be repulsive interactions whose strength is proportional to the size of the overlap.

Prior to any contact with a wall, however, a single droplet flowing through a hopper follows a simple differential equation. The equation of motion for a freely falling droplet in equilibrium is

$$mg = c\dot{y}. \tag{4.1}$$

Where m is the mass of the droplet, g is free fall acceleration due to gravity, c is a measure of viscosity and $\dot{y}$ is the time derivative of y position, i.e. the vertical velocity.

For wall interactions, the Durian bubble model has two different regions corresponding to the distance of the droplet from the exit, which I will denote by the terms inside and outside the painted area, shown in Fig.4.1. The circle is outside the paint when the position of the circle is between $w/2 < y < \sqrt{2}R - w/2$. The circle is inside the paint when the position lies

between $w/2 > y > -\sqrt{R^2 - (w/2)^2}$. Otherwise, the circle moves under free fall conditions.

For the region outside the paint, the overlap between the droplet and wall induces a normal reaction with a magnitude determined by the overlap length as such:

$$F_y^{out\ paint} = -\frac{k}{\sqrt{2}}(R - s). \tag{4.2}$$

Where k is a spring force constant that determines the characteristic strength of the repulsion between wall and droplet, R is the radius of the droplet, and s is the distance from the center of the droplet to the wall, given by $s = \frac{1}{\sqrt{2}}(y + w/2)$, where w is the width of the opening. Under equilibrium conditions, where the net force on the circle is $F_{net} = 0$ our equation of motion becomes:

$$\dot{y} + \nu y + \epsilon = 0 \tag{4.3}$$

Where $\nu = \frac{k}{c}$ and $\epsilon = \frac{w\nu}{2} - \sqrt{2}\nu R - \frac{mg}{c}$ are constants introduced for tidiness. Eq.4.3 has a decaying solution given by:

$$y(t) = \sqrt{2}R - \frac{w}{2} + \frac{mg}{k}(1 - e^{-\nu t}). \tag{4.4}$$

While this equation is easy to solve, its solution is relatively uninteresting compared to the dynamics inside the paint. More interestingly, for the region inside the paint, the wall-droplet repulsion force no longer points perpendicular to the droplet because such a line no longer exists perpendicular from the wall to the center of the droplet. The Durian bubble model models the wall force inside the paint as such:

$$F_y^{in\ paint} = -k \sin\theta (R - s). \tag{4.5}$$

Where θ is the angle made by the center of the droplet and the pincer of the hopper, and this force emanates solely from the pincer, whereas outside the paint moved the location of

the force along the wall. The distance from the center of the droplet to the wall is given by $s = \frac{y}{\sin\theta}$. From geometry, $\sin\theta = \frac{y}{\sqrt{(w/2)^2+y^2}}$. Gathering these formulas, the equation of motion becomes:

$$\dot{y} + \mu y + \tau - \frac{R\mu y}{\sqrt{(w/2)^2 + y^2}} = 0. \tag{4.6}$$

Where $\mu = \frac{2k}{c}$ and $\tau = \frac{-mg}{c} = v_T$, such that we achieve a form similar to Eq.4.3, with a non-linear correction. While the correction makes this differential equation difficult to solve, we can intuit a few properties. First, the velocity of the droplet at $y = 0$ is $v = \frac{mg}{c} = v_T$. When the droplet is halfway through the hopper, the Durian bubble model predicts that the droplet has been accelerated back to terminal velocity.

In addition, the sign of the correction flips as the center of the droplet switches from above to below the hopper. This means that this term at first works against the droplet's motion, pushing it upward, as we expect when a droplet confronts a constriction which forces the droplet to economise its energy in a different way. But, once the half the droplet has been pushed through by the brute force of gravity, the repulsive interaction between wall and droplet now aids in helping push the droplet out. As we can see in Fig.4.2, this repulsive interaction pushes the droplet out so much so that it overshoots its terminal velocity. Once the droplet reaches a certain distance the linear term starts to dominate again, meaning that the viscous drag slows the velocity back to terminal velocity. Then, the droplet is out of contact and moves under free fall conditions.

Since Eq.4.6 accounts for the presence of the overshoot, we can determine where this overshoot occurs by looking for the maximum velocity as a function of the position. Doing this tells us that:

$$y_{os} = -\sqrt{\left[R\left(\frac{w}{2}\right)^2\right]^{2/3} - \left(\frac{w}{2}\right)^2}. \tag{4.7}$$

Where y_{os} is the location of the overshoot. Immediately, this tells us that the overshoot disappears when $R = w/2$, also known as $w/d = 1$, where we expect no wall interactions, or

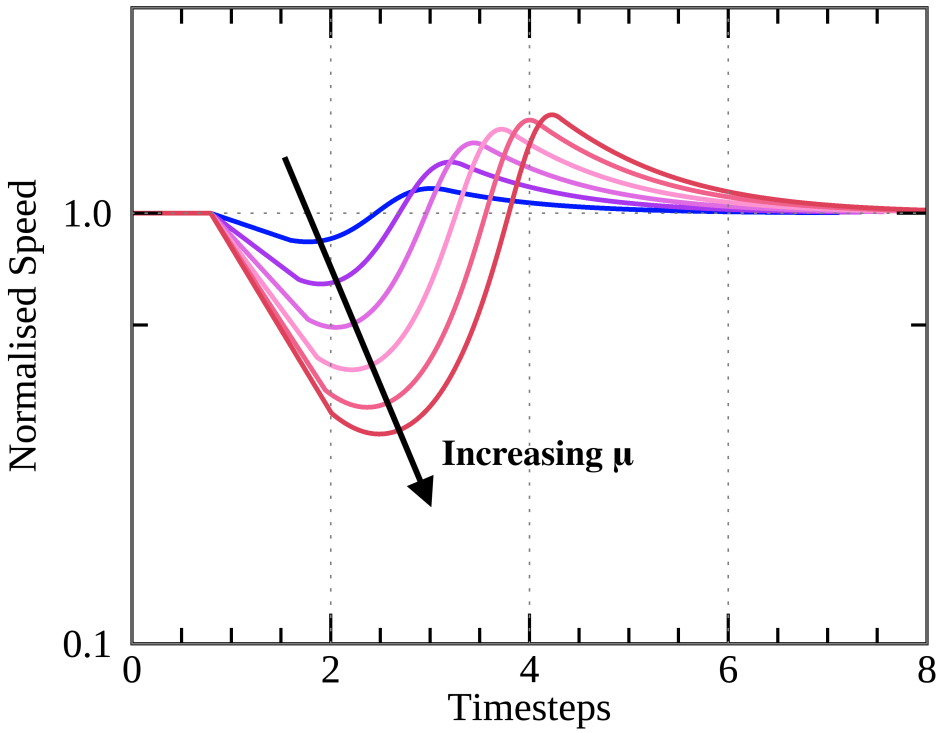

Figure 4.2: Graph of normalised speed (velocity divided by terminal velocity) against timesteps for a single droplet flowing through hopper over multiple values of μ. The blue curve represents the smallest value of μ, red the largest, and the colors in between increment μ by a factor of 10. Eq.4.6 tells us that the velocity at $y = 0$ is the terminal velocity. As such, the first intersection between the dotted line at Normalised Velocity $= 1$ and the velocity curve denotes the moment when the droplet is halfway through.

when $w/d = 0$, and the droplet is blocked from flowing.

We can also substitute y_{os} back into Eq.4.6 to quantify how the overshoot depends on the stiffness and drag of droplets. Doing this gives us that ratio of the overshoot to terminal velocity is:

$$\frac{\dot{y}_{os}}{v_T} = \frac{2ky_{os}}{mg}\left[\left(\frac{2R}{w}\right)^{2/3} - 1\right] + 1 \tag{4.8}$$

What we see here is that the size of the overshoot relative to the terminal velocity increases as k, the stiffness of the particles, also increases. This makes sense— stiffer particles are repelled by the wall more strongly, meaning that the droplet is *more* repelled by the wall such that the force of ejection is greater. What is interesting here is that the ratio of the velocities is not dependent on drag. This is a bit counter intuitive, as we would expect that stronger

drag means that energy is dissipated into the fluid so that the particle has less energy set aside for overshooting. But, we can reconcile this with the idea that stronger viscous dissipation means that the particle has a lower terminal velocity, such that the overshoot velocity must be compensating proportionally. This occurs because a slower terminal velocity results in a more sustained contact with the walls, such that it "feels" the repulsive interaction with greater sensitivity.

That said, when we can notice two limit cases that drive the overshoot to 0: either the viscous drag goes to infinity, in which case our terminal velocity goes to 0, or when the spring repulsion of the walls goes to 0, in which case the droplet and walls have no interaction. Thus, we recuperate, in some way, our intuition that drag and velocity are inversely proportional. Moreover, these two scenarios predict that the overshoot only disappears in trivial cases where the droplet cannot be considered to be flowing through an orifice. As a definitive statement: *the Durian bubble model predicts that the velocity overshoot exists for all cases where the droplet flows through the hopper.*

We have to be somewhat careful here not to be so adherent to the Durian bubble model that we delimit the phenomenon observed now out of some blind necessity for correspondence. After all, the Durian bubble model was first formulated to study the effect of shearing foams. Its recent application in hopper work has proven useful. But, these situations were not looking at regimes of extreme droplet deformation. Most important in this respect is that the Durian bubble model *does not* conserve the area of the droplets— any overlap between droplet and wall is a loss to the overall area of the droplet. As such, we are suspicious of these claims, but nonetheless looking to explore their characteristics, and through this exploration of extremely deformed droplets we can examine how this lack of a conservation manifests in the phenomenon of one particle flow.

4.1.2 Surface Energy and Velocity

We can also think about this problem from an energy perspective. Namely, the overshoot can be recast as a feature of how the droplet must deform in order to pass through the narrow opening. This deformation *away* from the circular shape costs surface energy. The deformation back *toward* a circle, however, releases surface energy. As such, once half the droplet has run through the hopper, any movement in the direction of gravity is also a step towards achieving a more circular shape, since the region above the hopper has the open space for the droplet to expand into. For this reason, if we assume that viscous dissipation is small relative to surface energy, then all surface energy at the velocity overshoot has been converted into kinetic energy as such:

$$U_s = \frac{1}{2}m(\dot{y}_{os}^2 - v_T^2). \tag{4.9}$$

For this reason, $\dot{y}_{os} \approx \sqrt{U_s^2 + v_T^2}$, and by extension $\dot{y}_{os}/v_T \approx \sqrt{1 + \left(\frac{U_s c}{mg}\right)^2}$, where U_s houses the information about how rigid our system is.[1]This casting of our overshoot recuperates many of the same proportionalities we discovered in the Durian bubble model. But it also leaves open the idea that if our surface energy, U_s, is less than our equal to the viscous dissipation energy, then there will not be enough surface energy to overshoot the velocity. The question remains, however, is there some intermediary range of parameters in which the viscous dissipation removes the overshoot *without* dissipating the energy needed for the droplet to move through the constriction?

4.1.3 Center of Mass Velocity

To test these predictions, I begin by looking at the time evolution of droplet velocity and deformation, shown in Fig.4.3.

I measure the deformation of droplets by calculating the ratio between perimeter squared

[1]Thank you to Yuxuan Cheng for showing me this other way of accounting for the overshoot.

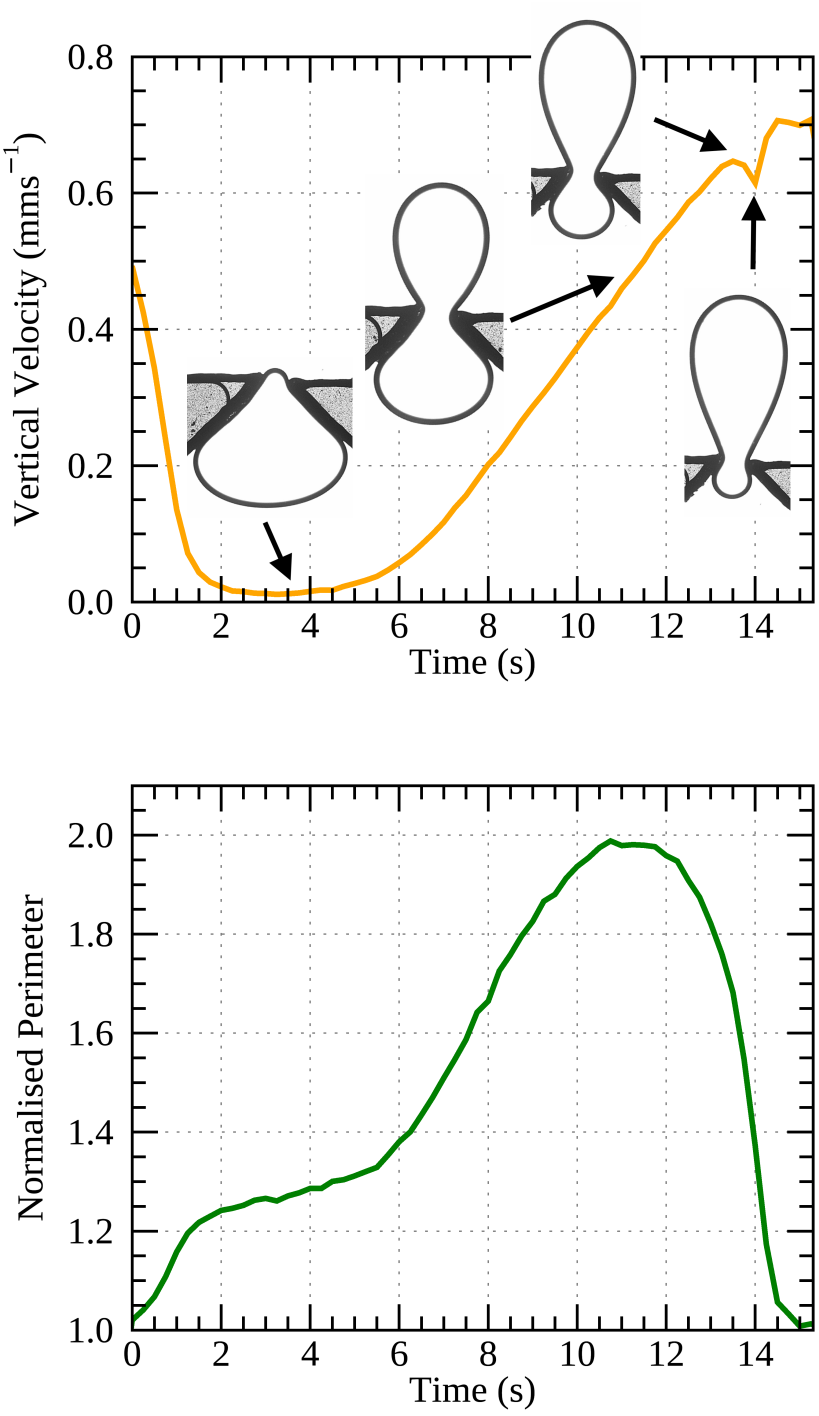

Figure 4.3: Graphs of velocity and normalised perimeter for a single droplet flowing through hopper. The data is taken for the same droplet, but averaged over the 6 trials.

to the area (times some normalisation constants), called the normalised perimeter, as such: $NP = \frac{\text{perimeter}^2}{4\pi \times \text{area}}$. Deformation is ultimately a measure of how far a droplet is from its most desired shape: a circle. Now, oil is incompressible, which means that its area is constant since its density is as well. This means that any deformation occurs within the stretching of the perimeter. In short, normalised perimeter measures the deviation of a droplets current perimeter to its perimeter if it were a perfect circle— any disconnect means that the perimeter of the current droplet has been stretched or compressed. Physically, any stretching or compressing is an energy cost in surface energy. Note the fact that increases in perimeter result in a greater exposed boundary, which means a greater exposed surface between the two fluids; the very thing surface energy wants to minimise. As such, normalised perimeter is our route to surface energy.

In Fig.4.3 we notice some predicted and obvious features. The droplet slows down when it reaches the wall, before speeding up as it moves through the hopper, eventually returning to its terminal velocity which we briefly encounter at the end. The initial slow down of the droplet, almost to $v = 0$, occurs as the droplet takes the shape of the wall. Once the droplet has molded to the shape of the hopper, it begins to go through, reaching its max deformation of nearly $NP = 2$ (meaning that the actual perimeter has been stretched by almost $1.4\times$ the length of the circular perimeter), whereupon it rapidly retakes its circular shape.

I also notice that the time for the droplet to reach the halfway point is slower than the time for the droplet to depart from the halfway point. I also notice a dip that occurs in the velocity near the exit.

The Durian bubble model says that this asymmetry is a consequence of the mutual repulsion between droplet and wall now pointing in the direction of gravity. In correspondence with this switch, the Durian bubble model predicts the presence of an overshoot. In the experiment, however, I observe this stunted overshoot in all one bubble trials. In fact, looking at the experimental data alone, we have little reason to call it an overshoot, since it remains safely below terminal velocity. As such, I prefer to call it a local velocity maximum.

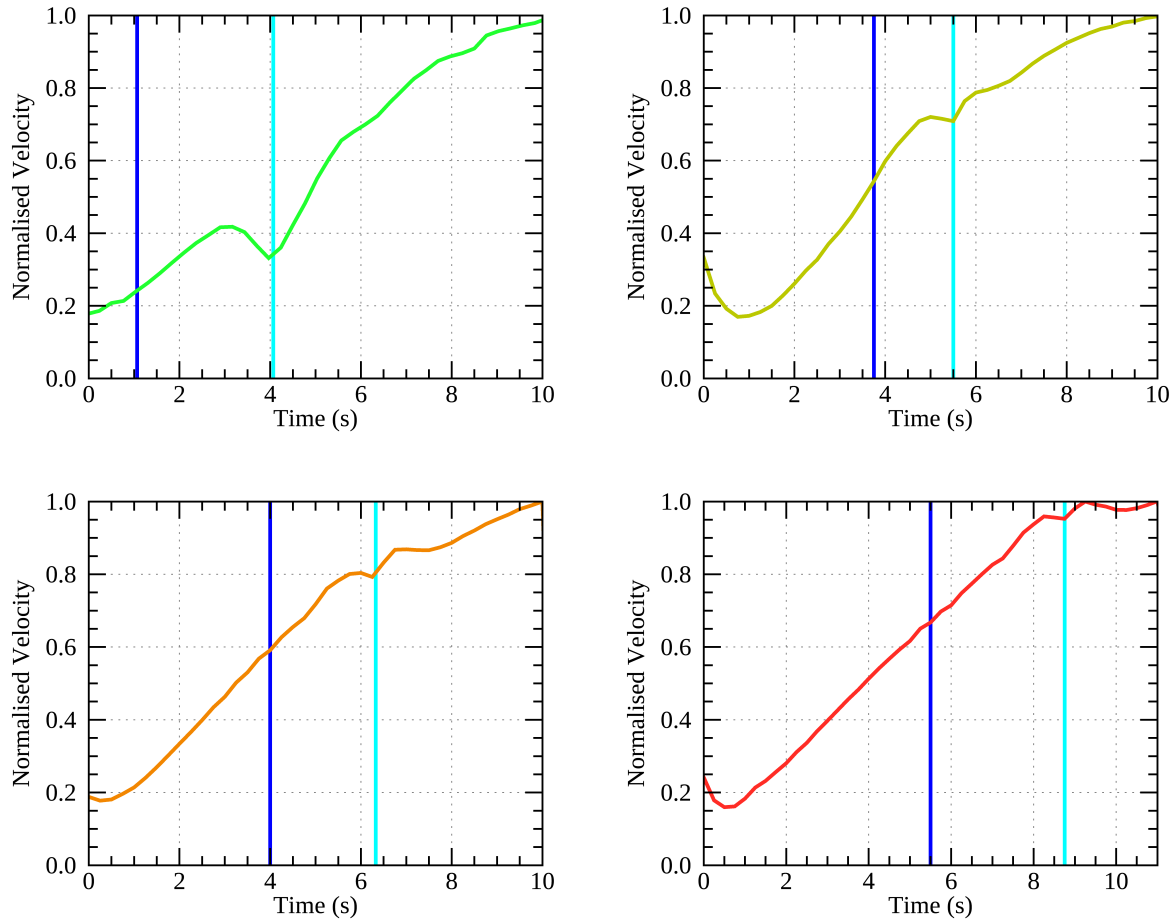

Figure 4.4: Graph of velocity as a function of time for four different values of w/d. The dark blue line represents when the droplet has a position of $y = 0$ relative to the hopper and the cyan line represents when the droplet stops making contact with the hopper. w/d decreases from top left to bottom right, from $w/d = 0.93$, $w/d = 0.51$, $w/d = 0.41$, to $w/d = 0.33$. The opening width is kept at the same value of $w \sim 900\mu m$.

In Fig.4.4 I plot the center of mass velocity for 4 different values of w/d. There are two notable features we mentioned briefly, but appear more robustly for varying diameters. 1) The presence of a local velocity maximum that occurs far below terminal velocity 2) The velocity of the droplet after departing from the hopper is below terminal velocity.

In these graphs we see that increasing the diameter of the droplet decreases the size of the local velocity maximum. For the largest radius size, in fact, we see that the local velocity maximum is barely visible, resembling a plateau more than any dip.

If we were to presuppose that the local velocity maximum corresponds to the predicted

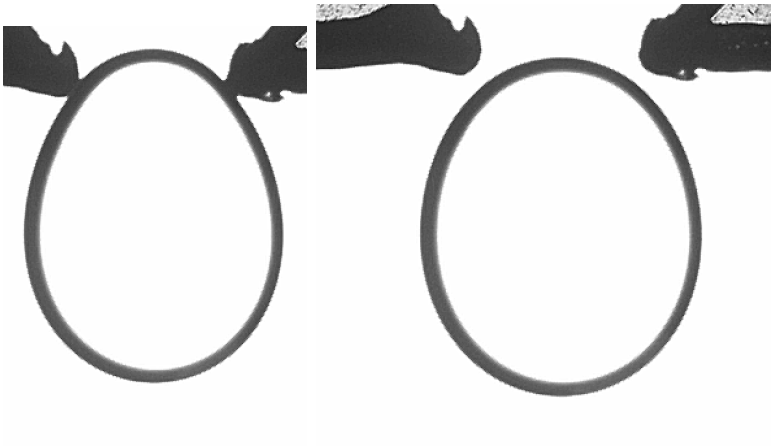

Figure 4.5: Consecutive image of droplet separating from wall. This separation corresponds to the timing for the local velocity minimum.

overshoot, then our read on this trend would be as follows: we know that smaller droplets are more rigid, corresponding to an increased k from Eq.4.6 and Eq.4.3, corresponding to an increased amplitude of overshooting. To be sure, shrinking the radius means shrinking the volume of oil and thus the strength of the buoyancy, but our overshoot term in Eq.4.3 is independent of the volume of oil. Indeed, *if* we thought this way, we would find agreement between the SP model and the experiment for the effect of surface tension on the size of the overshoot.

We were never certain of this thinking, and our decision to call this local velocity maximum a velocity overshoot is far too hasty. Another idea for what occurs in the local velocity maximum requires that we observe, with equal importance, the adjacent velocity minimum. Doing this, we see that the local velocity minimum occurs in frames when the droplet separates from the wall, as seen in the transition between consecutive frames in Fig.4.5. This suggests an adhesion between the walls and the droplet. One of the most famous adhesive interactions for this system is called the depletion force, the same depletion force we have already described.

If the slow down that occurs in the center of mass velocity is generated by the depletion force, then we must be very careful so as to not enforce the overshoot predicted by the SP model. For instance, this suggests that the local velocity maximum we see in the experiments

is not an overshoot at all but rather a *slow down* of the droplet from its trajectory. And our fixation on the local velocity maximum obscured the ability to understand that this *maximum* was derivative from the local velocity *minimum*. As such, this places the velocity curve in greater continuity with itself such that the curve, in the absence of depletion, would have a more sigmoidal shape, erasing the observed overshoot. For comprehension, but by no means accuracy, I have plotted a velocity curve with an overlaid with a sigmoidal fit in Fig.4.6.

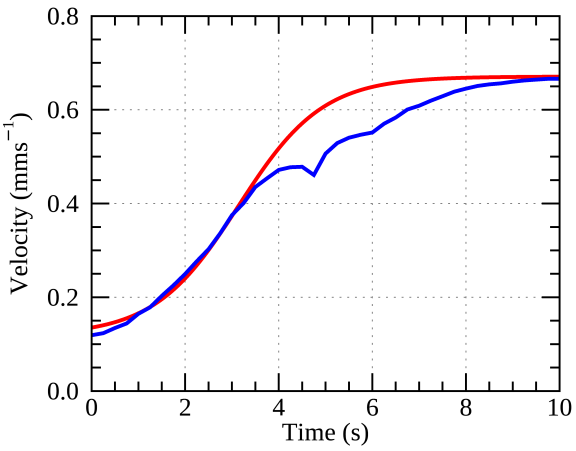

Figure 4.6: Speculation of velocity in the absence of depletion force. The blue curve is the actual velocity for a droplet of $d = 1578\mu m$ flowing through an opening width of $w = 821\mu m$ ($w/d = 0.52$). The red curve is a speculation for the velocity of the droplet in the absence of depletion, fitted to a sigmoidal function. Note the absence of the overshoot.

This idea is further supported by the fact that the slow down strengthens as the radius of the droplet decreases. Smaller radius means less volume, means less buoyancy, means that the depletion force can take on a more dominant role. Moreover, larger droplets not only have a stronger buoyant force, but their highly deformed character also tacks on a significant surface tension restoration, again suppressing the strength of the depletion force.

If this velocity slow down is a feature of the depletant, rather than evidence of an overshoot, a question remains as to whether the depletant erases the overshoot or whether *there never was one to begin with*. The former is what we have predicted from the SP model, whereas the latter is a case which our analysis of the differential form of the SP model asserted was impossible, but is shown as possible Fig.4.6. To be sure, the depletion force is at work whenever the contact between two surfaces is changed. For this reason, there would be an "unpeeling" effect at work as the droplet moves through the hopper. But, how does depletion dissipate energy relative to the overall energy of the droplet?

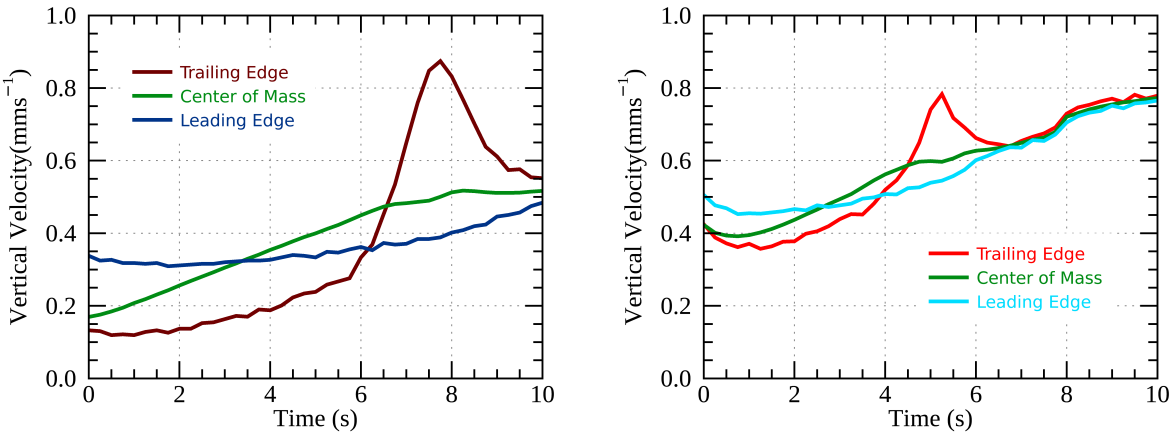

Figure 4.7: Graph of leading, trailing and center of mass velocity for two droplets. Red represents the trailing edge, blue represents the leading edge and green represents the center of mass. The right graph is for a droplet of size $d = 1.21mm$, an opening size of $d = 0.75mm$, and $w/d = 0.62$. The left graph is for a droplet of size $d = 2.44mm$, an opening size of $w = 0.80mm$, and $w/d = 0.33$. Note that The droplet goes out of frame before returning to circle in the left image.

4.1.4 Leading and Trailing Edge

To get a better sense for what happens in this local velocity minimum, and to gesture towards the metrics necessary in the study of extremely deformed droplets, I examine the velocity for the leading and trailing edge of the droplet. This idea emerges from the fact that our deformation parameter corresponds to a stretching or shrinking of the droplets perimeter from its desired circle shape. This stretching indicates that there is an imbalance in the velocity within the droplet— any time dependent deviation means that one side is moving faster than the other. Inversely, this means that a perfectly circular droplet will have identical leading and trailing edge velocity equal to the center of mass velocity.

By examining Fig.4.7 we see that the trailing edge initially runs slower than the leading edge. This corresponds to the droplet taking up the form of the hopper where the trailing edge is essentially stationary. Since a small volume of fluid moves through, this gives the leading edge a velocity. In this stage, the leading edge accounts for the center of mass velocity. This initial asymmetry in velocities is important because it accounts for how the droplet is deforming: the droplet deforms because the trailing edge of the droplet is held back by the

walls whereas the leading edge is propelled forward by its buoyancy. That is to say, taking reference from Fig.4.3, this taking shape corresponds to an increase in the deformation of the droplet, indicating a stretching that occurs along the perimeter of the droplet.

At the point of minimum velocity, however, the trailing edge of the droplet begins to accelerate faster than the leading edge. The velocity of the leading edge then sharply increases at the point when the droplet reaches its point of maximum deformation. This is likely due to the cooperation between gravity and surface tension where the droplet receives a reward for moving upward as well as becoming more circular. This sharp increase in the velocity of the trailing edge is then, with equal suddenness, cut short as the droplet exits the chamber.

The leading edge velocity lines up with the measured local velocity maximum, ultimately signalling that the local velocity maximum we measure in our experiments is driven by the velocity of the trailing edge of the droplet. Most importantly, this means that the local velocity maximum as well as the corresponding velocity minimum are arranged by the dynamics of what goes on at the trailing edge of the droplet. As such, that this sudden dip occurs along the trailing edge can provide evidence that the depletion force is at work, since only the trailing edge would be in greater proximity to the wall than the leading edge. Most importantly, the fact that the trailing edge velocity is sharp whereas the center of mass velocity is unresponsive signals a disconnect between the ability for the droplet to move as a group and the ability for the trailing edge to snap into shape. This suggests that in the absence of depletant the trailing, leading and center of mass velocities would meet each other rather than the trailing edge being stunted. That is, we expect the impetus of the trailing edge to push the entire droplet forward, especially for stiffer droplets.

A couple interesting features are of note in Fig.4.7. First, the point of maximum deformation corresponds to the crossover point between the leading and trailing edge velocities, which also aligns with the halfway point. Recalling that deformation corresponds to a stretching, the sharp increase in the leading velocity, as well as the moderate increase in the trailing edge velocity, that follows the decrease in deformation suggests that the velocity of the droplet is

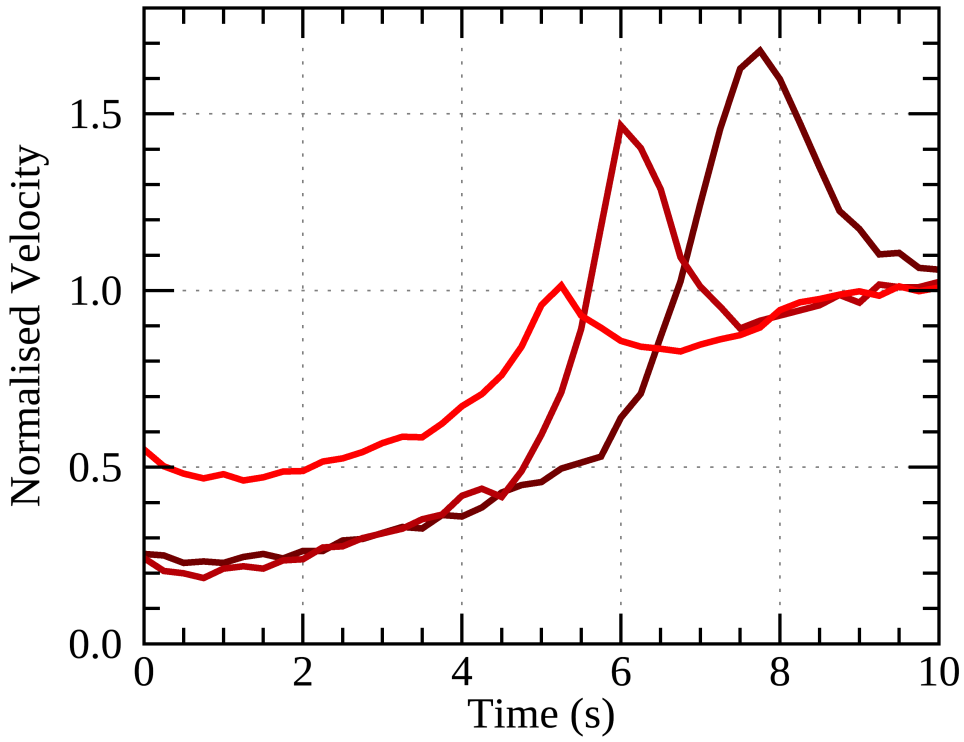

Figure 4.8: Graph of trailing edge velocity for three differently sized droplets. The diameter of the droplet increase as the shade of red goes darker. The smallest droplet has a diameter of $d = 1.21mm$, the medium sized droplet has a diameter of $d = 1.53mm$, and the large droplet has a diameter of $d = 2.44mm$. The opening width is relatively constant at $d \sim 0.8mm$

dominated by a springy surface tension which, in returning to its ideal shape, amounts to an increase in the velocity.

I also plot the trailing edge velocity for three different sizes of droplet, as shown in Fig.4.8. Looking at this graph, we can notice that the size of the trailing edge peak diminishes as we go to smaller droplets. This interesting because we would expect that because the deformation of smaller droplets cost more surface energy, the trailing edge would reconnect to the main body with greater speed. If we track, however, the *difference* between the leading and trailing edges from Fig.4.7, we notice that the smaller droplet holds these two together. This likely occurs because of the surface energy penalty for deformation away from a circle is greater for both a smaller diameter and the more rigid shape. For large droplets, which are more deformable, the penalty for stretching the droplet is small and the gravitational

reward for moving through is greater, in turn leading to a greater ability for the leading edge to "run ahead" of the trailing edge. As such, the larger trailing edge for the larger droplets corresponds to an ability for larger droplets to sustain large asymmetries in the velocity between the leading and trailing edge.

4.2 Summary of Findings

I have studied here the dynamics of one droplet flow through a hopper where the opening width, w, is smaller than the diameter, d. In doing this, I made reference to Durian bubble model as a leading computational model for soft particles, providing an analytic solution to how one Durian model droplet would move through an opening smaller than its diameter. This examination predicted the presence of a velocity overshoot where the wall-droplet repulsion ejects the droplet out of the hopper at a velocity greater than its terminal velocity. Alongside this model, I also presented an argument for the overshoot that appeals to energy conservation. This approach gave us the question as to whether viscous drag could dissipate energy such that the excess surface energy for overshooting was depleted without dissipating the energy needed for the droplet to flow through at all. Experimentally, I find the presence of a local velocity minimum, which I have argued could be a feature of the depletion force. I have speculated that it is possible that the viscosity of the fluid used in this experiment behaves in a regime of extreme droplet deformation outside the limits where the Durian bubble model can be applied. Furthermore, I have measured the asymmetric velocities across the droplet as a way of gesturing towards the metrics of interest in the study of more deformable droplets. This has shown that larger, and therefore softer, droplets are able to vary their velocities across the droplet, since the surface energy penalty for doing so is smaller.

Conclusion

My project here has looked at two similar, but inverted, situations. Both projects have been attempting to understand how the flow of soft, frictionless things differs from our general understanding of particle flow.

For multiple particles, I showed how the frictionless conditions of the experiment generated a flow that differs from flow where friction is the key dissipative mechanism, and that this slipperiness does not correspond neatly to an easing of flow, as we might expect if we were to take away a dissipative mechanism. Instead, the flow of soft droplets is slower than frictional systems. If we think more generally, this occurs because of the way that these two mechanisms, viscous drag and kinetic friction, dissipate energy. Friction dissipates energy only when two particles are in contact. Viscous dissipation is more global, always acting on the particle. This suggests that the impedance to flow for soft frictionless droplets is more "open" to viscous drag as we increase the opening size. In the study of soft particles, this result shows a need to think about how the dissipative mechanisms work in order to understand how these droplets flow.

I also study one particle flow in order to explore the limits of our traditional model for soft particles. Even before any quantitative statements, we can already glean from Fig.4.3 the insufficiency and inaccuracy in modelling this droplet as a circle. More importantly, by looking at the velocity of the droplet, and focusing on the velocity asymmetry in leading and trailing edges of the droplet, we can get a sense for how the droplet deforms as it interacts with obstacles and how this deformation is a feature of the surface penalty for exposed

boundaries. The dynamics of this deformation is interesting because it opens up avenues for exploring how the actual shape of the droplet can activate certain behaviours outside the scope delimited when we imagine droplets as circles with elastic potentials. Looking ahead, we can begin to think of scenarios which were encountered in this project as crises, such as droplet break up and coalescence. How would droplets flow if coalescence was activated? How might they flow if they can break up? Which would be favored?

In this concluding remark, I would like to point to what I believe to be an important, but neglected feature in the study of soft particle flow: the medium of flow. To be sure, the many particle system actively considered the viscosity of the fluid as co-determinant in the dynamics of the system. To do this, however, we had to toss out the regions of data where the background of the fluid was markedly non-static. Similarly, in the flow of one large particle the drag that the droplet feels would likely be different as the droplet travels through the hopper. Take, for instance, the images shown on Fig.4.3: a circular droplet is not as aerodynamic as the droplet while it squeezes through the opening, since the effective radius relative to viscous drag is markedly smaller.

Ultimately, what I mean by these final points is to motivate and demonstrate the necessity for modelling these droplets with an attunement to their physical dynamics, in order to study what makes them unique, rather than trying to assimilate them into the context of hard particles.

Bibliography

[1] Fernando Alonso-Marroquin and Peter Mora. Beverloo law for hopper flow derived from self-similar profiles. *Granular Matter*, 23, 02 2021. doi: 10.1007/s10035-020-01067-1.

[2] Solomon Barkley, Eric R. Weeks, and Kari Dalnoki-Veress. Snap-off production of monodisperse droplets. *The European Physical Journal E*, 38(12), dec 2015. doi: 10.1140/epje/i2015-15138-8. URL https://doi.org/10.1140%2Fepje%2Fi2015-15138-8.

[3] Yann Bertho, Christophe Becco, and Nicolas Vandewalle. Dense bubble flow in a silo: An unusual flow of a dispersed medium. *Phys. Rev. E*, 73:056309, May 2006. doi: 10.1103/PhysRevE.73.056309. URL https://link.aps.org/doi/10.1103/PhysRevE.73.056309.

[4] Wim A. Beverloo, H. A. Leniger, and Joris Van de Velde. The flow of granular solids through orifices. *Chemical Engineering Science*, 15:260–269, 1961.

[5] Arman Boromand, Alexandra Signoriello, Fangfu Ye, Corey S. O'Hern, and Mark D. Shattuck. Jamming of deformable polygons. *Phys. Rev. Lett.*, 121:248003, Dec 2018. doi: 10.1103/PhysRevLett.121.248003. URL https://link.aps.org/doi/10.1103/PhysRevLett.121.248003.

[6] Arman Boromand, Alexandra Signoriello, Janna Lowensohn, Carlos S. Orellana, Eric R. Weeks, Fangfu Ye, Mark D. Shattuck, and Corey S. O'Hern. The role of deformability in determining the structural and mechanical properties of bubbles and emulsions. *Soft*

Matter, 15:5854–5865, 2019. doi: 10.1039/C9SM00775J. URL http://dx.doi.org/10.1039/C9SM00775J.

[7] RL Brown. Minimum energy theorem for flow of dry granules through apertures. *Nature*, 191(4787):458–461, 1961.

[8] John C Crocker and David G Grier. Methods of digital video microscopy for colloidal studies. *Journal of colloid and interface science*, 179(1):298–310, 1996.

[9] John C Crocker and Brenton D Hoffman. Multiple-particle tracking and two-point microrheology in cells. *Methods in cell biology*, 83:141–178, 2007.

[10] D. J. Durian. Foam mechanics at the bubble scale. *Phys. Rev. Lett.*, 75:4780–4783, Dec 1995. doi: 10.1103/PhysRevLett.75.4780. URL https://link.aps.org/doi/10.1103/PhysRevLett.75.4780.

[11] Jianhua Fan, Li-Hua Luu, Pierre Philippe, and Gildas Noury. Discharge rate characterization for submerged grains flowing through a hopper using dem-lbm simulations. *Powder Technology*, 404:117421, 2022. ISSN 0032-5910. doi: https://doi.org/10.1016/j.powtec.2022.117421. URL https://www.sciencedirect.com/science/article/pii/S0032591022003151.

[12] Anisa Hofert. Flow of quasi-2d emulsion droplets through small openings. Bachelor's thesis, Emory University, 2020.

[13] Xia Hong, Meghan Kohne, Mia Morrell, Haoran Wang, and Eric R. Weeks. Clogging of soft particles in two-dimensional hoppers. *Phys. Rev. E*, 96:062605, Dec 2017. doi: 10.1103/PhysRevE.96.062605. URL https://link.aps.org/doi/10.1103/PhysRevE.96.062605.

[14] R.M. Nedderman, U. Tüzün, S.B. Savage, and G.T. Houlsby. The flow of granular materials—i: Discharge rates from hoppers. *Chemical Engineering Science*, 37(11):

1597–1609, 1982. ISSN 0009-2509. doi: https://doi.org/10.1016/0009-2509(82)80029-8. URL https://www.sciencedirect.com/science/article/pii/0009250982800298.

[15] Rhutesh K. Shah, Ho Cheung Shum, Amy C. Rowat, Daeyeon Lee, Jeremy J. Agresti, Andrew S. Utada, Liang-Yin Chu, Jin-Woong Kim, Alberto Fernandez-Nieves, Carlos J. Martinez, and David A. Weitz. Designer emulsions using microfluidics. *Materials Today*, 11(4):18–27, 2008. ISSN 1369-7021. doi: https://doi.org/10.1016/S1369-7021(08)70053-1. URL https://www.sciencedirect.com/science/article/pii/S1369702108700531.

[16] Daniel A. Steingart and James W. Evans. Measurements of granular flows in two-dimensional hoppers by particle image velocimetry. part i: experimental method and results. *Chemical Engineering Science*, 60(4):1043–1051, 2005. ISSN 0009-2509. doi: https://doi.org/10.1016/j.ces.2004.09.066. URL https://www.sciencedirect.com/science/article/pii/S0009250904007298.

[17] Ran Tao. Flow and clogging of soft particles in 2d hoppers. Bachelor's thesis, Emory University, 2021.

[18] Ran Tao, Madelyn Wilson, and Eric R. Weeks. Soft particle clogging in two-dimensional hoppers. *Phys. Rev. E*, 104:044909, Oct 2021. doi: 10.1103/PhysRevE.104.044909. URL https://link.aps.org/doi/10.1103/PhysRevE.104.044909.

[19] Andrew S. Utada, Alberto Fernandez-Nieves, Howard A. Stone, and David A. Weitz. Dripping to jetting transitions in coflowing liquid streams. *Phys. Rev. Lett.*, 99:094502, Aug 2007. doi: 10.1103/PhysRevLett.99.094502. URL https://link.aps.org/doi/10.1103/PhysRevLett.99.094502.

[20] Jing Wang, Bo Fan, Tivadar Pongó, Kirsten Harth, Torsten Trittel, Ralf Stannarius, Maja Illig, Tamás Börzsönyi, and Raúl Cruz Hidalgo. Silo discharge of mixtures of soft and rigid grains. *Soft Matter*, 17:4282–4295, 2021. doi: 10.1039/D0SM01887B. URL http://dx.doi.org/10.1039/D0SM01887B.

[21] T. J. Wilson, C. R. Pfeifer, N. Mesyngier, and D. J. Durian. Granular discharge rate for submerged hoppers. *Papers in Physics*, 6:060009, Oct. 2014. doi: 10.4279/pip.060009. URL https://www.papersinphysics.org/papersinphysics/article/view/212.

[22] Xia Xin, Hongxing Zhang, Guiying Xu, Yebang Tan, Jian Zhang, and Xin Lv. Influence of ctab and sds on the properties of oil-in-water nano-emulsion with paraffin and span 20/tween 20. *Colloids and Surfaces A: Physicochemical and Engineering Aspects*, 418: 60–67, 2013. ISSN 0927-7757. doi: https://doi.org/10.1016/j.colsurfa.2012.10.065. URL https://www.sciencedirect.com/science/article/pii/S0927775712007601.